The Visual System of a Palaeognathous Bird: Visual Field, Retinal Topography and Retino-Central Connections in the Chilean Tinamou (*Nothoprocta perdicaria*)

Quirin Krabichler,[1]* Tomas Vega-Zuniga,[1] Cristian Morales,[2] Harald Luksch,[1]* and Gonzalo J. Marín[2,3]*

[1]Chair of Zoology, Technische Universität München, Freising-Weihenstephan, Germany
[2]Laboratorio de Neurobiología y Biología del Conocer, Departamento de Biología, Facultad de Ciencias, Universidad de Chile, Santiago de Chile, Chile
[3]Facultad de Medicina, Universidad Finis Terrae, Santiago de Chile, Chile

ABSTRACT

Most systematic studies of the avian visual system have focused on Neognathous species, leaving virtually unexplored the Palaeognathae, comprised of the flightless ratites and the South American tinamous. We investigated the visual field, the retinal topography, and the pattern of retinal and centrifugal projections in the Chilean tinamou, a small Palaeognath of the family Tinamidae. The tinamou has a panoramic visual field with a small frontal binocular overlap of 20°. The retina possesses three distinct topographic specializations: a horizontal visual streak, a dorsotemporal area, and an area centralis with a shallow fovea. The maximum ganglion cell density is 61,900/ mm^2, comparable to Falconiformes. This would provide a maximal visual acuity of 14.0 cycles/degree, in spite of relatively small eyes. The central retinal projections generally conform to the characteristic arrangement observed in Neognathae, with well-differentiated contralateral targets and very few ipsilateral fibers. The centrifugal visual system is composed of a considerable number of multipolar centrifugal neurons, resembling the "ectopic" neurons described in Neognathae. They form a diffuse nuclear structure, which may correspond to the ancestral condition shared with other sauropsids. A notable feature is the presence of terminals in deep tectal layers 11–13. These fibers may represent either a novel retinotectal pathway or collateral branches from centrifugal neurons projecting to the retina. Both types of connections have been described in chicken embryos. Our results widen the basis for comparative studies of the vertebrate visual system, stressing the conserved character of the visual projections' pattern within the avian clade. J. Comp. Neurol. 523:226–250, 2015.

INDEXING TERMS: retinal ganglion cells; retinal projections; centrifugal visual system; isthmo-optic nucleus; optic tectum; avian; deep tectal pathway; RRID: AB_10013220

As a group, birds rank among the most visual vertebrates that ever lived on earth. Their reliance on vision is manifested in very large eyes and a highly differentiated visual system, in which the visual pathways and nuclei, conforming to a common vertebrate neural *Bauplan*, are particularly distinct and well developed (Güntürkün, 2000; Karten, 1969).

However, in spite of large-scale comparative studies exploring the allometric variations of specific brain structures (Corfield et al., 2012; Iwaniuk et al., 2005, 2010), systematic anatomical and electrophysiological investigation of the avian visual system has focused on only few species: the chicken (*Gallus gallus*; Ehrlich and Mark, 1984a,b; Koshiba et al., 2005; Luksch et al., 2001; Verhaal and Luksch, 2013; Wang et al., 2004, 2006), the

Grant sponsor: Chilean National Fund for Scientific and Technological Development (FONDECYT); Grant number: 1110281.

*CORRESPONDENCE TO: Quirin Krabichler, Lehrstuhl für Zoologie, Technische Universität München, Liesel-Beckmann Strasse 4, 85354 Freising-Weihenstephan, Germany. E-mail: quirin.krabichler@tum.de; Harald Luksch, Lehrstuhl für Zoologie, Technische Universität München, Liesel-Beckmann Strasse 4, 85354 Freising-Weihenstephan, Germany. E-mail: harald.luksch@wzw.tum.de; and Gonzalo J. Marín, Laboratorio de Neurobiología y Biología del Conocer, Facultad de Ciencias, Universidad de Chile, Las Palmeras 3425, Ñuñoa, Santiago, Casilla 653, Chile. E-mail: gmarin@uchile.cl

Received April 25, 2014; Revised September 5, 2014;
Accepted September 9, 2014.
DOI 10.1002/cne.23676
Published online September 16, 2014 in Wiley Online Library (wileyonlinelibrary.com)

rock pigeon (*Columba livia*; Benowitz and Karten, 1976; Binggeli and Paule, 1969; Karten et al., 1973, 1997; Letelier et al., 2004; Marín et al., 2003, 2012; Mpodozis et al., 1995; Remy and Güntürkün, 1991; Shimizu et al., 1994), the quail *(Coturnix coturnix*; Budnik et al., 1984; Ikushima et al., 1986; Maturana and Varela, 1982; Norgren and Silver, 1989a), the barn owl (*Tyto alba*; Bravo and Pettigrew, 1981; Gutfreund, 2012; Gutfreund et al., 2002; Harmening and Wagner, 2011; Knudsen, 2002; Pettigrew and Konishi, 1976; Wathey and Pettigrew, 1989), and the zebra finch (*Taeniopygia guttata*; Bischof, 1988; Faunes et al., 2013; Keary et al., 2010; Schmidt and Bischof, 2001; Schmidt et al., 1999); all of them pertaining to the Neognathae, the grand clade to which most extant bird species belong.

Modern birds, or Neornithes, however, include a second extant clade, the Palaeognathae (Hackett et al., 2008), encompassing six living families: Struthionidae (ostrich), Dromaiidae (emu), Casuariidae (cassowaries), Apterygidae (kiwi), Rheidae (rheas), and Tinamidae (tinamous) (Harshman et al., 2008). Surprisingly, apart from a few studies (e.g., on the retinal topography of the ostrich [Boire et al., 2001; Rahman et al., 2010], on the photoreceptors of ostrich and rhea [Wright and Bowmaker, 2001], or on the sensory systems of the kiwi [Martin et al., 2007]), the Palaeognathae have been vastly ignored by comparative neurobiologists, even though their considerable phylogenetic distance from the commonly studied Neognathae — 120–130 million years (Brown et al., 2008; Haddrath and Baker, 2012) — makes them a very interesting subject for gaining insights into the evolution of the avian visual system and the scale of the phylogenetic plasticity of its constituent elements.

Undoubtedly, the lack of attention toward palaeognathous birds can be largely explained by their scarcity and, not least, by their difficult manageability: most Palaeognaths are rather large, fierce animals, such as the ostrich or the emu, whereas the smaller kiwis exhibit highly derived characteristics with a greatly reduced visual system (Martin et al., 2007).

However, there is one palaeognathous group without such drawbacks: The Tinamiformes, consisting of the sole family Tinamidae, represent 47 species in nine genera (Bertelli and Porzecanski, 2004; Bertelli et al., 2014), which are endemic to the Neotropics of South and Middle America (Cabot, 1992). They are diurnal birds, and are generally medium-sized (the largest about the size of a pheasant). Intriguingly, they are the only living Palaeognathae that can fly. Even so, they are ground-dwelling birds and make use of their short but strong wings only to escape from immediate danger or to reach their roost (Cabot, 1992; Conover, 1924; Pearson and Pearson, 1955). This remarkable lifestyle suggests well-developed sensory capacities, particularly in the visual system, and especially in those tinamous inhabiting open terrains, the Steppe tinamous (subfamily Nothurinae; Bertelli et al., 2014).

Figure 1. The Chilean tinamou (*Nothoprocta perdicaria*) in the wild. Lateral view and frontal portrait (inset). Photography by Sergio Bitran M. [Color figure can be viewed in the online issue, which is available at wileyonlinelibrary.com.]

In the present study, as a first step in an overall investigation of the visual system of a Steppe tinamou, the Chilean tinamou (*Nothoprocta perdicaria*; Fig. 1), we mapped the extent of the visual field, examined the topography of the retinal ganglion cell layer (GCL) and, by injecting cholera toxin subunit B (CTB) into the eye, traced the retinal connections to the central targets in the brain.

MATERIALS AND METHODS

Seven adult Chilean tinamou (*Nothoprocta perdicaria*) were used in this study. They were acquired from a Chilean breeder (Tinamou Chile, Los Ángeles, Chile). The animals were kept in cages with food and water *ad libitum*. All efforts were made to minimize animal suffering, and experiments were conducted in compliance with the guidelines of the U.S. National Institutes of Health on the use of animals in experimental research, with the approval of the bioethics committee of the Facultad de Ciencias of the Universidad de Chile.

Measurement of the visual field

The visual field measurements were conducted by the methods described in Vega-Zuniga et al. (2013). Four animals were anesthetized with a mixture of ketamine (120 mg/kg IP) and xylazine (4 mg/kg IP) and mounted in a stereotaxic head holder in the center of a custom-built campimeter. The head was positioned so that the palpebral fissures were aligned with the campimeter's equator (analysis of photographs of

relaxed birds showed that the normal posture of the head is inclined downward by approximately 10° relative to this position). During the experiment, the eyelids of the birds were held open with thin strips of masking tape, and the eyes were kept constantly moist by applying sterile NaCl solution every few minutes. We then used an ophthalmoscopic reflex technique to measure the visual fields of both eyes of each bird, determining the nasal and temporal limits of the retinal reflections and noting the angles in a conventional latitude/longitude coordinate system.

Retinal whole-mounts

For analysis of the retinal whole-mounts, we followed the methods described by Ullmann et al. (2012). The eyes of three animals were enucleated from their sockets after phosphate-buffered saline (PBS) perfusion of the animals (see below), their axial length was measured with digital calipers, and they were hemisected close to the ora serrata. The vitreous body was removed from each retina, which was then dissected from the sclera, ending with the excision of the optic nerve head and pecten. With forceps and fine paintbrushes, the retina was cleared from the pigment epithelium and, after flattening with four radial incisions, was whole-mounted on gelatin-coated slides, left to dry and firmly attach to the gelatin, and fixed overnight with paraformaldehyde (PFA) vapors at 60°C. Afterward, the retina was Nissl-stained, dehydrated in ascending alcohols followed by clearing in xylene, and cover-slipped with DPX (Sigma-Aldrich Chemie, Steinheim, Germany). No assessment was made of possible areal shrinkage of the retina, which is reportedly minimal in whole-mounted retinas affixed to gelatin-coated slides (Wässle et al., 1975).

Retinal cross sections

Two Chilean tinamou eyes were removed immediately after perfusion of the animal (see below), hemisected at the ora serrata (see Fig. 4A), and postfixed for 6 hours in 4% PFA. The eyecups were then transferred into a 30% sucrose/PBS (0.1 M: 0.023 mM NaH_2PO_4 and 0.08 mM Na_2HPO4, pH 7.4; with NaCl 0.75%) solution until they sank. A gelatin embedding solution was produced by adding 10 g sucrose and 12 g gelatin type A (Sigma-Aldrich Chemie) to 100 ml $H_2O_{dest.}$ and heating it to 55°C to dissolve the gelatin. Both the eyecups in sucrose solution and the gelatin solution were put into an oven at 37°C until they reached the same temperature. Then the vitreous bodies were removed from the eyecups, which were subsequently embedded in gelatin. The gelatin–eyecup blocks were trimmed, and put into 4% PFA for postfixation for 2–5 hours and afterward into 30% sucrose/PBS for cryoprotection until they sank. They were sectioned with a cryostat (Kryostat 1720, Leica, Wetzlar, Germany) at 30 μm in both the transversal and horizontal planes, and the sections were mounted on gelatin-coated slides, Nissl-stained, rapidly dehydrated in ascending alcohols followed by clearing in xylene, and cover-slipped with DPX.

Visual acuity estimation of the eye

The maximal spatial resolving power (SRP) was approximated using the sampling theorem (Hughes, 1977). This is a way to estimate the theoretical maximal visual acuity from the eye's posterior nodal distance (PND) and the peak density of retinal ganglion cells (RGCs) (Collin and Pettigrew, 1989; Pettigrew et al., 1988; Ullmann et al., 2012). The inclusion of non-ganglionic cell populations (i.e., displaced amacrine cells) in the estimation is negligible because of the

Abbreviations

AC	area centralis
AOS	accessory optic system
AP	area pretectalis
APd	area pretectalis, pars dorsalis
CO	optic chiasm
cpd	cycles per degree
CTB	cholera toxin subunit B
DAB	diaminobenzidine
DLAmc	n. dorsolateralis anterior thalami, pars magnocellularis
DLL	n. dorsolateralis anterior thalami, pars lateralis
DTA	dorsotemporal area
EC	ectopic cell
ECR	ectopic cell region
GCL	retinal ganglion cell layer
GLv	n. geniculatus lateralis, pars ventralis
GLd	n. geniculatus lateralis, pars dorsalis
GT	tectal gray
IGL	intergeniculate leaflet
ION	isthmo-optic nucleus
LA	n. lateralis anterior thalami
LdOPT	n. lateralis dorsalis optici principalis thalami
LM	n. lentiformis mesencephali
LMl	n. lentiformis mesencephali, pars lateralis
LMm	n. lentiformis mesencephali, pars medialis
nBOR	n. of the basal optic root
nIV	nucleus nervi trochlearis
nMOT	n. marginalis tractus optici
OT	optic tract
PBS	Phosphate-buffered saline
PFA	paraformaldehyde
PND	posterior nodal distance
PT	n. pretectalis
RGC	retinal ganglion cell
ROI	region of interest
Rt	n. rotundus
SO	stratum opticum
SPC	n. superficialis parvocellularis
SpRt	n. suprarotundus
SRP	spatial resolving power
Tdp	deep tectal pathway
TeO	optic tectum
TIO	isthmo-optic tract
vSCN	visual suprachiasmatic nucleus
VLT	n. ventrolateralis thalami

relatively very small ratio of such cells in high-density retinal areas (Hayes and Holden, 1983). Because no direct measurement of the PND was made, the known approximate PND to axial length ratio of 0.60 in diurnal birds was used as described in the literature (Boire et al., 2001; Hughes, 1977; Martin, 1993; Ullmann et al., 2012): PND=0.60 × axial length. The angle covering 1 mm on the retina is then: $\alpha = \arctan \frac{1\ mm}{PND}$. Spatial resolution is estimated by calculating the number of cells covered by 1 degree of visual arc in the area centralis (AC). Because the cell density is given in cells/mm^2, the square root is applied to convert it to cells/mm. The number of cells per degree is: *cells per degree* $= \frac{density\ at\ area\ of\ peak\ cell\ distribution}{\alpha}$. Finally, the result has to be divided by 2, because at least two cells are necessary for one cycle of grating (one light and one dark bar in one degree of visual angle). Thus, the SRP is given in *cycles per degree* (cpd): $SRP\ [cpd] = \frac{cells\ per\ degree}{2}$.

Neuronal tracing experiments

For the intraocular tracer injection experiments, five birds were sedated and anesthetized with a mixture of 4% halothane and oxygen, delivered at a constant flow of 1 L/min using a customized mask placed around the bill.

The skin dorsal to the eye socket was incised with a scalpel to expose the eyeball. A small cut was made in the dorsal sclera, through which CTB (20 µl of ~0.83% in PBS with 2% dimethylsulfoxide [DMSO]; List Biological, Campbell, CA) was injected into the eye's vitreous body with a Hamilton (Reno, NV) syringe. After the procedure, the skin wound was closed with instant adhesive and treated with antiseptic povidone–iodine solution.

The birds were then allowed to recover. After survival periods of 5–7 days, the animals were deeply anesthetized and perfused intracardially with PBS and subsequently 4% PFA (in PBS). The brains were dissected from the skull, postfixed in 4% PFA, and transferred into a 30% sucrose/PBS solution until they sank.

The brains were sectioned in the transversal plane with a cryostat or a freezing microtome at a section thickness of 50 µm, collected in PBS, and alternately separated into three or four series for subsequent anti-CTB immunohistochemistry. The sections were immersed in 90% methanol/3% H_2O_2 for 10 minutes to quench endogenous peroxidase activity, and incubated overnight with a primary polyclonal anti-CTB antibody raised in goat (List Biological, cat. no. 703, RRID: AB_10013220; diluted 1:40,000 in PBS/0.3% Triton X-100/5% normal rabbit serum). After a subsequent 1-hour incubation with a secondary biotinylated anti-goat IgG (H+L) antibody raised in rabbit (Vector, Burlingame, CA; diluted 1:1,500 in PBS/0.3% Triton X-100), ABC solution (avidin–biotin peroxidase complex; Vectastain Elite ABC Kit, Vector) was added to bind to the biotinylated secondary antibodies. In a final step, the ABC peroxidase activity was used for diaminobenzidine (DAB) precipitation by incubating the sections for 6 minutes in a 0.025% DAB/0.0025% H_2O_2 solution (using DAB-buffer tablets for microscopy; Merck, Darmstadt, Germany) in imidazole–acetate buffer/1% $NiSO_4$ for intensification and contrast enhancement (Green et al., 1989).

Processed sections were mounted on gelatin-coated slides, counterstained according to standard Nissl or Giemsa protocols or left clear ("CTB plain"), and coverslipped with DPX after dehydration in ascending alcohol series and clearing in xylene.

Stereology

Retinal whole-mounts

Microscopic examination and photographing of the histological material were performed under an Olympus BX63 microscope with an attached DP26 digital color camera (Olympus, Tokyo, Japan).

Four retinal whole-mounts (two right eyes and two left eyes) were analyzed. The Nissl-stained ganglion cells were counted live by using the microscope software CellSens Dimension v1.7 (Olympus Soft Imaging Solutions, Münster, Germany). Using a ×60 water immersion objective, cell counting was performed according to the fractionator principle (Gundersen, 1977) in regions of interest (ROIs) sampled at regular intervals, while using the focus control in order to better differentiate cells from one another.

To define the ROIs and draw the retinal GCL isodensity maps, we took photomicrographs of the entire Nissl-stained retinal whole-mounts (stitched together by the microscope software), projected them onto the wall with a beamer, and drew their contours onto graph paper at a scale of 20:1. The ROI positions were defined by a 2 × 2-cm grid on the graph paper, which thus corresponded to a 1 × 1-mm grid on the true-scale retinal whole-mount. The respective coordinates of each grid point were targeted with the motorized microscope stage, and at each position an ROI of 100 × 100 µm was defined in the software as an unbiased counting frame (Gundersen et al., 1988b). According to this principle, we only counted neurons within the ROI or touching the ROI frame at two out of four sides (the other two being the adjacent "exclusion edges"). RGCs could be easily distinguished from the small, spindle-shaped glial cells (Wathey and Pettigrew,

1989), which were disregarded in the counting, but distinction from displaced amacrine cells by cytological criteria (Ehrlich, 1981) would only have been feasible in areas of low cell densities. Therefore, we decided not to distinguish between RGCs and displaced amacrine cells, and all our data presented here include displaced amacrine cells, but not glial cells.

Cell counts were filled into the hand-drawn retina map, which was then digitalized with a scanner. In Photoshop CS5 (Adobe Systems, San Jose, CA), isodensity contours were drawn to visualize the cell distribution of the GCL across the retina. Furthermore, the total cell number in the GCL was estimated by assuming mean cell densities for the isodensity areas and multiplying those values by the respective areas in mm^2, according to the following model (Vega-Zuniga et al., 2013):

$$N_{total} = \sum_{i=1}^{n} A_i \; \bar{d}_i \begin{cases} \bar{d}_i = \left(\dfrac{d_{inner} + d_{outer}}{2} \right), & i \geq 2 \\ \bar{d}_i = d, & i = 1 \end{cases}$$

where A_i are the isodensity areas, $\bar{d}_i$ the respective mean densities, and d_{inner}, d_{outer} the cell densities for the isodensity contours confining each area, respectively.

Retinal cross sections

Because of the high density of neurons in the GCL, a modified optical disector method (Hatton and Von Bartheld, 1999) was applied to remedy the problem of bias due to differential shrinkage in frozen nervous tissue sections (Carlo and Stevens, 2011). Under the microscope using a ×60 water immersion objective and differential interference contrast (DIC), RGCs were counted in 30-µm-thick retinal cross sections across the whole section thickness in a 33.3-µm-long (x-axis; parallel to the GCL) counting frame with an exclusion edge on one side (Gundersen, 1977; Gundersen et al., 1988a,b). In the y-axis no exclusion edge was necessary, because the GCL was counted in its full width (see Fig. 4). An exclusion surface was defined in the uppermost focal plane of the section by only counting Nissl-stained perikarya coming into best focus below it. By these rules, counting was performed at 13 random positions around and within the foveal depression in three adjacent sections containing the AC. The numbers thus acquired resembled the numbers of cells/999 μm^2 of retinal surface (30 × 33.3 µm), respectively, and their mean was converted to cells per 1 mm^2 by multiplication with 1,001.

Estimation of centrifugal neurons

The total number of centrifugal neurons in the dorsal isthmic region was estimated by using an unbiased optical fractionator stereology approach (West, 1999; West et al., 1991), similar to the method previously described (Gutiérrez-Ibáñez et al., 2012). In the histological material of one tinamou, all sections of one out of four series (i.e., every fourth section) that contained retrogradely labeled neurons were analyzed by randomly superimposing a 0.01-mm^2 square grid, and defining an unbiased counting frame (Gundersen, 1977) of 0.05 × 0.05 mm^2 at each grid node. At each counting frame position, the section thickness was measured with the microscope focus, and guard zones were established at the upper and lower surface to account for sectioning irregularities. The guard zones were defined so that the z-space in between them had a known fraction of the section thickness (about 2/3), such that a cuboid was formed under the counting frame. This counting cuboid was unbiased in that three adjacent sides of it served as "exclusion edges" and the other three as "inclusion edges" (Gundersen et al., 1988a). Neurons were counted when their perikarya came into focus residing inside the cuboid or touching one of the inclusion sides and not touching any of the exclusion sides. Furthermore, the mean diameters of all counted cell profiles ($n = 180$ contralateral, $n = 14$ ipsilateral) were measured in the microscope software.

Coefficients of error (CEs) for the retinal cross section as well as the centrifugal neurons counts were calculated with Scheaffer's equation (Schmitz and Hof, 2000).

RESULTS

Visual field measurements

Figure 2 depicts the results from the ophthalmoscopic visual field analysis. Because the results from all eight eyes measured were highly similar (with the standard deviations at each coordinate mostly far below 10°, and in the frontal binocular visual field always below 4°), we show only one representative case. The Chilean tinamou possesses a maximum frontal binocular overlap of 20° (Fig. 2A,B), which is located about 13° above the line connecting the pupil with the tip of the bill (Fig. 2A). The overlap extends some 80° from above to below, with its biggest (and generally broader) field above the bill tip. The bill's projection falls amid the binocular field. Within the horizontal plane (Fig. 2B), the tinamou has, in addition to the binocular overlap, a monocular field of 140° (thus, each eye has a field of 160°). The blind sector to its rear measures 60°. Altogether, the bird has a panoramic visual field of 300°.

Eye morphology, retinal topography, and regional specializations

Five enucleated eyes were measured with a digital caliper. The axial length (AL) was 10.68 ± 0.43 mm, the

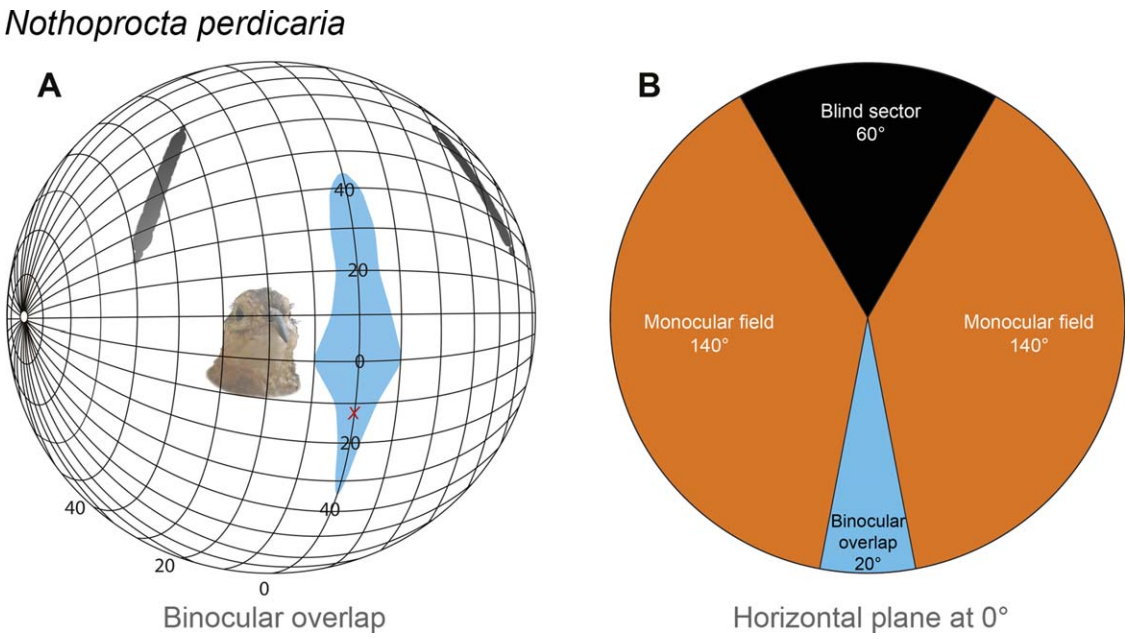

Figure 2. Visual field and binocular overlap. **A:** Perspective view of an orthographic projection of the tinamou's frontal binocular visual field and the pectens. The maximum binocular overlap is approximately 20° azimuth (conventional latitude/longitude system). The tip of the bill points toward −13° latitude (cross), and is completely encompassed by the binocular overlap. **B:** Plan view of the azimuthal plane through the visual field along 0° latitude. [Color figure can be viewed in the online issue, which is available at wileyonlinelibrary.com.]

transverse diameter 14.79 ± 0.25 mm, and the corneal diameter (CD) 6.26 ± 0.41 mm. The "eye shape," the $\log_{10}$ of the CD:AL ratio (Hall and Ross, 2007), was −0.232. The three flat-mounted retinal whole-mounts analyzed had an average area of 257.1 ± 4.3 mm^2. Stereological analysis of the Nissl-stained GCL allowed us to estimate the quantity of neurons in the GCL and reveal the topographical specializations of the Chilean tinamou retina. The total number of neurons in the GCL was estimated at 4.3 ± 0.2 × 10^6. The average neuron density across the entire retinal surface is thus 16.8 ± 0.8 × 10^3 neurons/mm^2.

Drawing isodensity contours with predefined thresholds revealed three types of retinal topographical specializations. Because all three retinal topography maps were very congruent, we show only one representative map (Fig. 3). Close to the center lies a high-density area centralis (AC; Fig. 3C), slightly nasally to the optic disk and pecten oculi. The maximum RGC density estimated in this region is 61.9 ± 2.3 × 10^3 RGCs/mm^2, more than 3.5 times the average neuron density in the retina. Dorsally and slightly temporally to this area, there is a broad dorsotemporal area (DTA; Fig. 3B) of high neuron density between 30 and 40 × 10^3 neurons/mm^2, which is segregated from the AC by a narrow part of lower neuron density. A horizontal visual streak extends nasally and temporally from the AC, dorsal to the pecten. It is of slightly lower neuron density than the DTA, ranging from 20 to 30 × 10^3 neurons/mm^2. Insets in Figure 3 illustrate the scope of variation in GCL neuron density and RGC morphology, which occurs across different topographical areas of the retina. In the outer, low-density periphery (Fig. 3A), the RGCs tend to be larger and fewer than in the high-density areas (e.g., AC or DTA).

Retinal cross-section structure

We made retinal cross-sections for two distinct reasons. First, microscopy of the whole-mounts suggested that in high-density areas the RGCs were stacked over one another, which compromised the achievement of confident cell counts in such regions. We reasoned that we could test our results by applying optical dissector stereology to cross sections. Second, in the whole-mounts it was not possible to ascertain whether the AC of the Chilean tinamou retina contained a true fovea or not. Freshly dissected retinae appeared to have a moderate depression at this position with a slightly different color, visible under a stereomicroscope (Fig. 4A). Therefore, we sectioned two retinae at 30 μm, one transversally and one horizontally, and studied the central region in more detail.

Figure 4B depicts a transverse section at the level of the AC, which is located dorsal to the nasal portion of the optic nerve head (compare Fig. 3). Because we had prepared the complete section series, and another one in

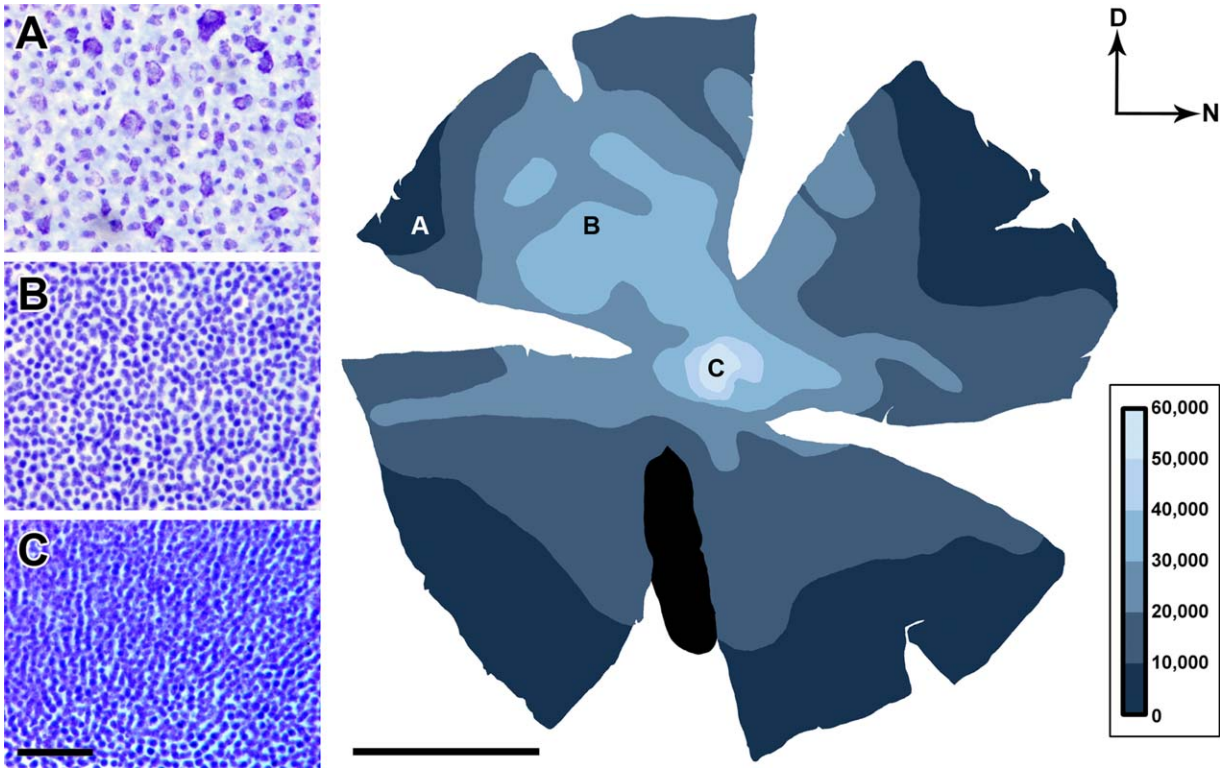

Figure 3. Topographical distribution of neurons in the retinal ganglion cell layer (GCL).The shaded scale on the right indicates the neural density within the respective isodensity contours (in cells/mm^2). Insets on the left show photomicrographs of Nissl-stained regions at representative positions: near the border (**A**), in the dorsotemporal area (**B**), and in the area centralis (**C**), demonstrating the substantial density differences within the GCL. The black patch marks the position of the pecten. Dorsal is up and nasal is to the right (as indicated by arrows). Scale bar = 50 μm in C (applies to A–C); 5 mm in topography map to the right. [Color figure can be viewed in the online issue, which is available at wileyonlinelibrary.com.]

the horizontal plane, we could ascertain that the section shown passes through the very center of the AC, showing the clearest representation of the depression. As the inset of the AC (Fig. 4C) shows, the depression can be distinguished in the GCL and all subsequent layers down to the outer nuclear layer (ONL), except for the inner and outer segments of the photoreceptors (IS + OS). Thus, the Chilean tinamou retina appears to possess a concaviclivate fovea, although shallow and little pronounced.

In the AC, the GCL is approximately 25–30 μm thick and contains five to six stacked layers of RGCs, which appear to be organized in a gross columnar fashion. A similar organization can be seen in the inner nuclear layer (INL), which contains densely packed bipolar, amacrine and horizontal cells. It has a pronounced thickness, ranging from 100 to 125 μm in the perifoveal region. In regions of lower cell densities, the stacking decreases and the columnar organization vanishes (Fig. 4C–E). Accordingly, the other retinal layers (INL, ONL, and the photoreceptor segments [IS + OS]) are less thick in regions of lower RGC density (Fig. 4D,E), with the exception of the inner plexiform layer (IPL), which in the DTA is even thicker than in the AC (100–105 vs. 60–80 μm).

Our stereological analysis of the AC in the GCL cross sections (see Materials and Methods) yielded 58.1 ± 2.3 × 10^3 RGCs/mm^2 of retinal surface (CE = 0.0109). If only samples in the center of the foveal depression were taken into account, the estimation was slightly lower (57.6 ± 2.4 × 10^3 RGCs/mm^2 of retinal surface; CE = 0.0337); in the case of all samples except those in the fovea, it was slightly higher (58.4 ± 2.5 × 10^3 RGCs/mm^2 of retinal surface; CE = 0.0081).

SRP estimation

The theoretical maximum of visual acuity (i.e., the SRP) was estimated from the eye's axial length and RGC density in the AC (see Materials and Methods). Because the focal length of the tinamou eye was not directly measured, the evaluation is partly based on the assumption that there is a constant PND to axial length ratio of 0.6 in birds (Hughes, 1977; Martin, 1993; Ullmann et al., 2012). The focal length was thus estimated at 6.41 mm. As described above, two different values

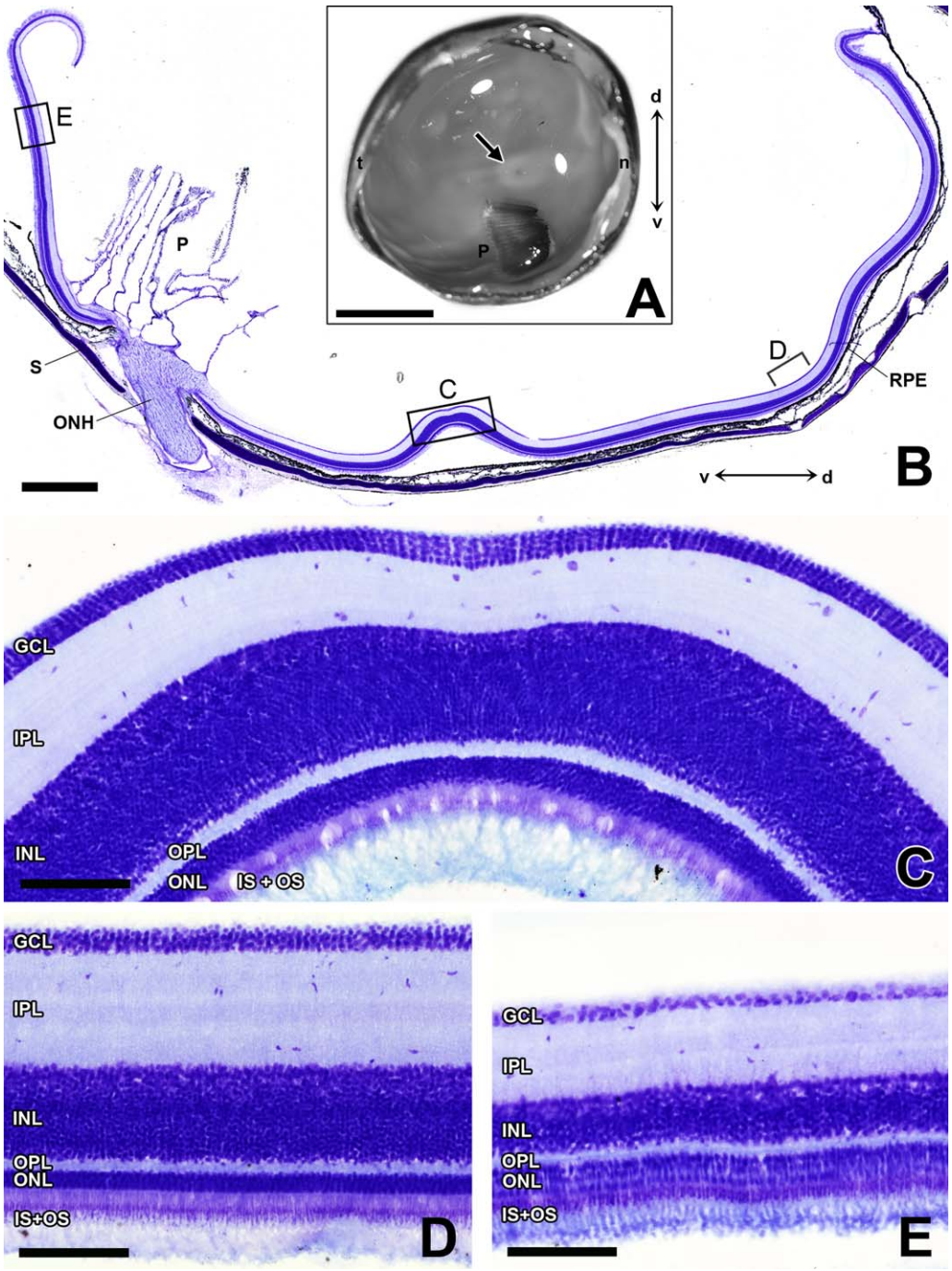

Figure 4. The retinal structure and the shallow fovea of the tinamou. **A:** Photo of a hemisected eyecup (same orientation as in Figure 3; n = nasal, t = temporal). The central fovea (arrow) is clearly visible as a small depression located dorsal to the pecten. **B–E:** Nissl-stained transverse sections (30 μm) of the retina displaying the retinal laminae; from inner to outer: ganglion cell layer (GCL), inner plexiform layer (IPL), inner nuclear layer (INL), outer plexiform layer (OPL), outer nuclear layer (ONL), and the inner (IS) and outer segments (OS) of the photoreceptors. **B:** Overview of a section through the area centralis and the optic nerve head (ONH) with the pecten (P) attached. Sclera (S) and retinal pigment epithelium (RPE). **C:** Enlarged view of a section through the middle of the area centralis (as marked in B). Note the shallow fovea manifested as a small depression in the GCL and INL, and the pronounced thickness of the retinal layers. The ganglion cells form stacks of about five to six cells. The elevation of the retina in the central aspect is an artefact due to a wrinkle in the retina formed by detachment from the retinal pigment epithelium (RPE) during fixation. **D:** Detail of dorsotemporal area. The layers are generally thinner than in the area centralis (except for the IPL, which is thicker), and the GCL contains notably fewer neurons. **E:** Detail of the GCL near the ventral border of the retina. Note that most layers are thinner, the photoreceptor segments are much shorter, and the ganglion cells are scarcer and larger. Scale bar = 5 mm in A; 1 mm in B; 100 μm in C–E. [Color figure can be viewed in the online issue, which is available at wileyonlinelibrary.com.]

of the maximum RGC density in the AC were obtained: The retinal whole-mount analysis yielded $61.9 \pm 2.3 \times 10^3$, and the cross-section three-dimensional stereology $58.3 \pm 1.3 \times 10^3$ RGCs/mm^2. Using both values resulted in SRP estimations of 14.0 and 13.6 cycles/degree, respectively.

The Chilean tinamou brain

The dissected brain of the adult Chilean tinamou (Fig. 5) measures approximately 2 cm in length from the tip of the olfactory bulb to the posterior end of the medulla. The three birds used for the tracer experiments weighed between 386 and 540 g (442 ± 85 g), and their brains weighed 1.93 ± 0.12 g after perfusion and postfixation. These values lie amid those of related tinamou species, and also the allometric relation of body weight to brain weight falls in line with other Tinamidae (Corfield et al., 2008). The Chilean tinamou brain's shape is roughly similar to a pigeon or chicken brain. The visual Wulst of the telencephalon is fairly conspicuous from the outside, and the lobe of the optic tectum (TeO) is well developed and relatively large.

Primary visual projections

Transverse section series with various counterstaining procedures (Nissl, CTB Nissl, CTB Giemsa) or with plain anti-CTB immunohistochemistry were produced of the five available Chilean tinamou brains with intraocular injections of CTB. Retinal terminals were found in all retinorecipient areas known from neognathous birds: in the dorsal and the ventral thalamus, the hypothalamus, the pretectum, the tectum, and the accessory optic system (Figs. 6–9). The vast majority of retinal afferents made a complete decussation at the chiasma opticum (Figs. 6, 7) and were therefore confined to the contralateral hemisphere (with respect to the eye that had received the tracer injection). Careful scrutiny also revealed sparse ipsilateral fibers and terminals, which were found in some dorsal thalamic, pretectal, and AOS structures (see below), but not at all in the TeO.

Dorsal thalamus

The well-known components of the avian dorsolateral geniculate (GLd) complex (classically also called the *nucleus opticus principalis thalami* [OPT]) receive a substantial retinal input (Figs. 7C,D, 8A). In the *n. dorsolateralis anterior thalami, pars lateralis* (DLL), the largest nucleus of the GLd complex, the retinal terminals were distributed exclusively into its ventral portion (Figs. 7C,D, 8A). The *n. dorsolateralis anterior thalami, pars magnocellularis* (DLAmc), which could be delimited from the laterally adjoining DLL by its slightly larger cells, received very few retinal fibers, mostly confined to its anterior ventral part (Fig. 8A). The *n. lateralis dorsalis optici principalis thalami* (LdOPT) appeared heavily innervated by retinal fibers, where they formed large terminal clusters, very distinct from other retinorecipient zones (Fig. 8A). Although this nucleus was difficult to distinguish from the adjacent DLL in plain Nissl material, it appeared as a very well-defined nucleus when the retinal projections were visualized. Another dorsal thalamic structure clearly receiving retinal terminals was the *n. suprarotundus* (SpRt; Fig. 8A). Retinal fibers without terminals were further seen in the *n. superficialis parvocellularis* (SPC; data not shown).

As has been mentioned before, the vast majority of retinal projections to the GLd were confined to the

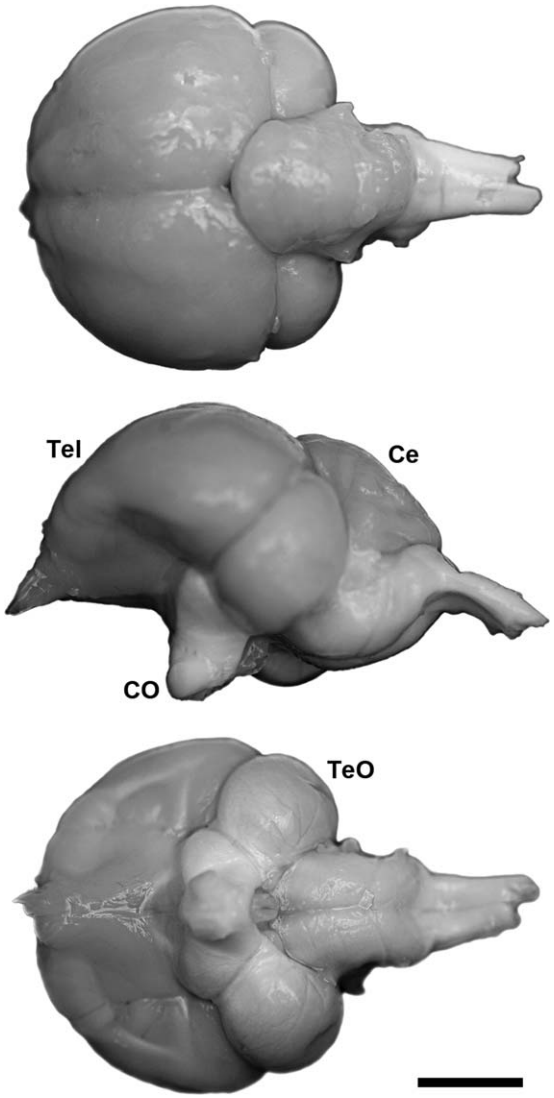

Figure 5. Photographs of the dissected brain. From dorsal (top), lateral (middle), and ventral (bottom). Ce, cerebellum; CO, chiasma opticum; Tel, telencephalon; TeO, optic tectum. Scale bar = 5 mm.

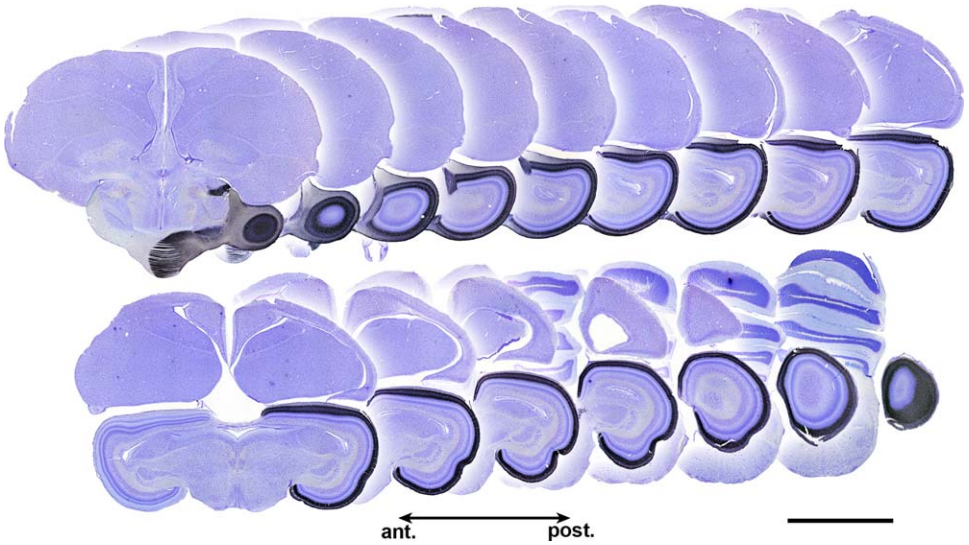

Figure 6. Projection pattern of retinal terminals in the contralateral optic tectum. Series of coronal Nissl-stained sections across the brain, demonstrating the contralateral retinal afferents to the TeO. The sections stem from one complete CTB-reacted series, presented at anteroposterior intervals of 400 μm. Note that the entire TeO is labeled, illustrating that the tracer was taken up by the whole extent of the retina. Scale bar = 5 mm. [Color figure can be viewed in the online issue, which is available at wileyonlinelibrary.com.]

contralateral hemisphere, but sparse terminals were also found in two ipsilateral GLd subunits: the DLL and the LdOPT (data not shown).

Ventral thalamus

As in all birds, the ventral thalamus of the Chilean tinamou is dominated by the *n. geniculatus lateralis, pars ventralis* (GLv; Figs. 7B–E, 8C). The GLv shows a laminated structure (Guiloff et al., 1987), with two clearly visible laminae: the *lamina interna* (GLv-li) with tightly packed somas receiving very sparse retinal afferents, and a neuropil layer (GLv-ne) with dense retinal terminals (Vega-Zuniga et al., 2014). Another nucleus of the avian ventral thalamus is the *n. lateralis anterior thalami* (LA), which showed a high density of retinal terminals (Figs. 7A,B, 8B). This nucleus appears very large in the tinamou compared with the pigeon, for example (Güntürkün and Karten, 1991). In addition, we found a low density of fibers and terminals in the *n. marginalis tractus optici* (nMOT; Figs. 7B–D, 8B) which, as in other birds, first appears at the rostral margin of the thalamus and continues to form an envelope around the LA (Güntürkün and Karten, 1991), and more caudally around the *n. rotundus* (Rt) just below the DLL. In the *n. ventrolateralis thalami* (VLT), which lies between the GLv and Rt and is a known retinorecipient region in birds (Schulte et al., 2006), we found only a few sparse terminals (Fig. 7D).

In terms of ipsilateral retinal projections in the ventral thalamus, we found only a few scattered terminals in the anterior portion of the LA (data not shown).

Hypothalamus

Retinal afferents to the hypothalamus were not very dense and terminated in a diffuse region at the dorsal border of the anterior optic tract (Figs. 7A,B, 9A). We could not differentiate between a lateral and a medial part as described in the pigeon (Shimizu et al., 1994). Instead, the projection pattern we found seemed to conform only to the lateral structure described there. Following the nomenclature put forward by Cantwell and Cassone (2006), we call it the visual suprachiasmatic nucleus (vSCN).

Pretectum and AOS

Several pretectal structures showed innervation from the retina (Figs. 7D,E, 9B): The *n. lentiformis mesencephali* (LM), which is divided into a medial (LMm) and a lateral (LMl) lamina (following the nomenclature by Gamlin and Cohen, 1988a,b; Pakan and Wylie, 2006; Pakan et al., 2006; Sorenson et al., 1989) juxtaposed between the ventral and dorsal strata optica medial to the TeO, showed very dense retinal innervation. Immediately lateral to the LM, a broad sheet with similarly dense retinal projections constitutes the tectal gray (GT). Other retinorecipient structures are found dorsally to the *n. pretectalis* (PT): Following the nomenclature of Gamlin and Cohen (1988a), these are the *area*

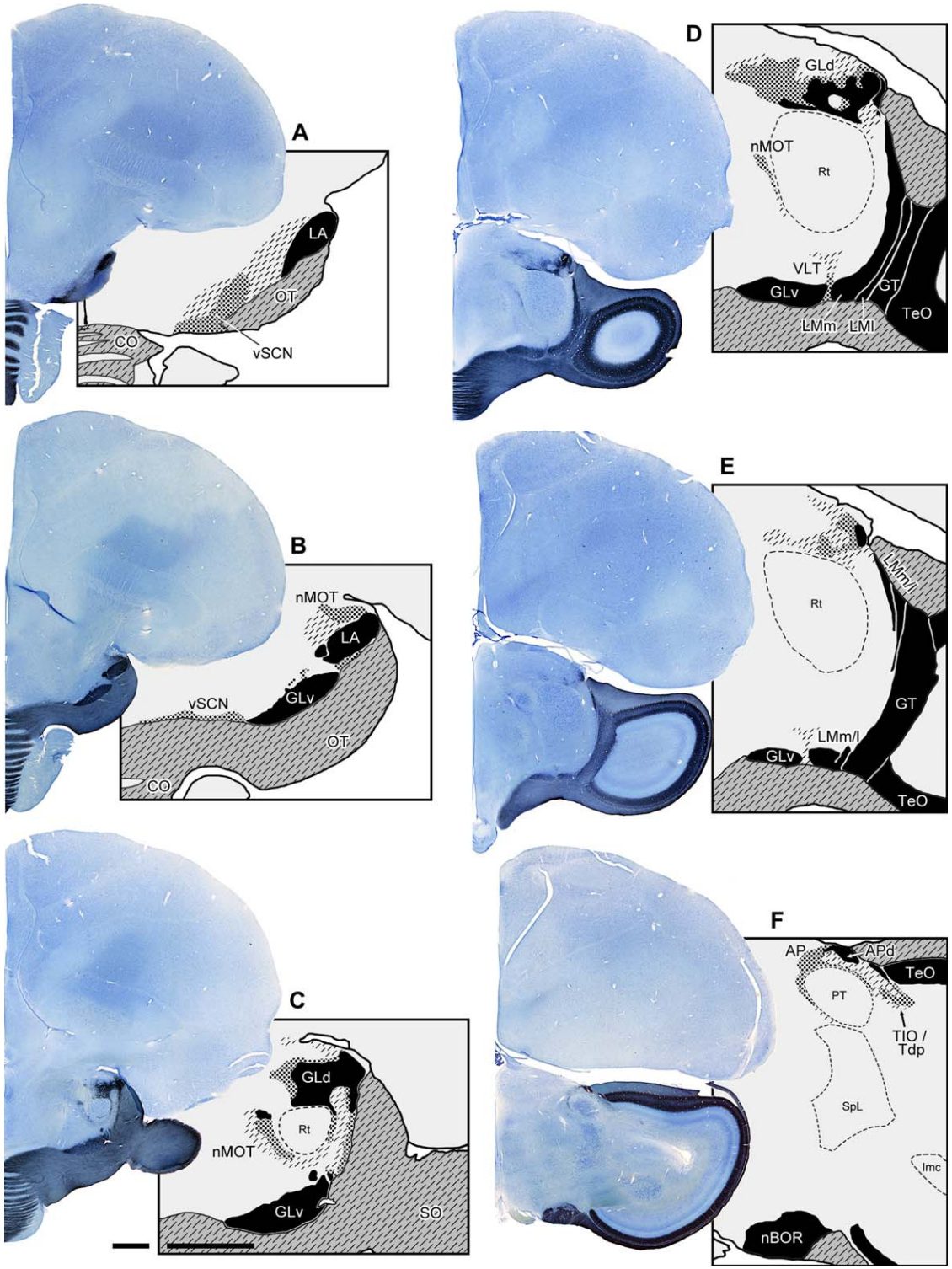

Figure 7. Overview of the retinal projections to central targets in the brain. **A–F:** Each panel displays a coronal section, counterstained with Giemsa, from rostral (A) to caudal (F), along with a corresponding schematic of the CTB-labeled retinal terminal fields. All typical target areas receiving contralateral retinal input are well-developed. They are observed in the hypothalamus (vSCN; A,B), the thalamic ventrolateral geniculate complex (LA, GLv; A–E) and adjoining regions (nMOT, VLT; B–D), the dorsolateral geniculate complex (GLd; C,D), the TeO (D–F), the pretectum (LMm, LMl, GT, AP, APd; D–F), and the accessory optic system (nBOR; F). Also visible is the centrifugal isthmo-optic tract (TIO; F), which includes the tract of the deep tectal pathway (Tdp; compare Fig. 11). For abbreviations, see list. Scale bars = 1 mm in C (apply to A–F). [Color figure can be viewed in the online issue, which is available at wileyonlinelibrary.com.]

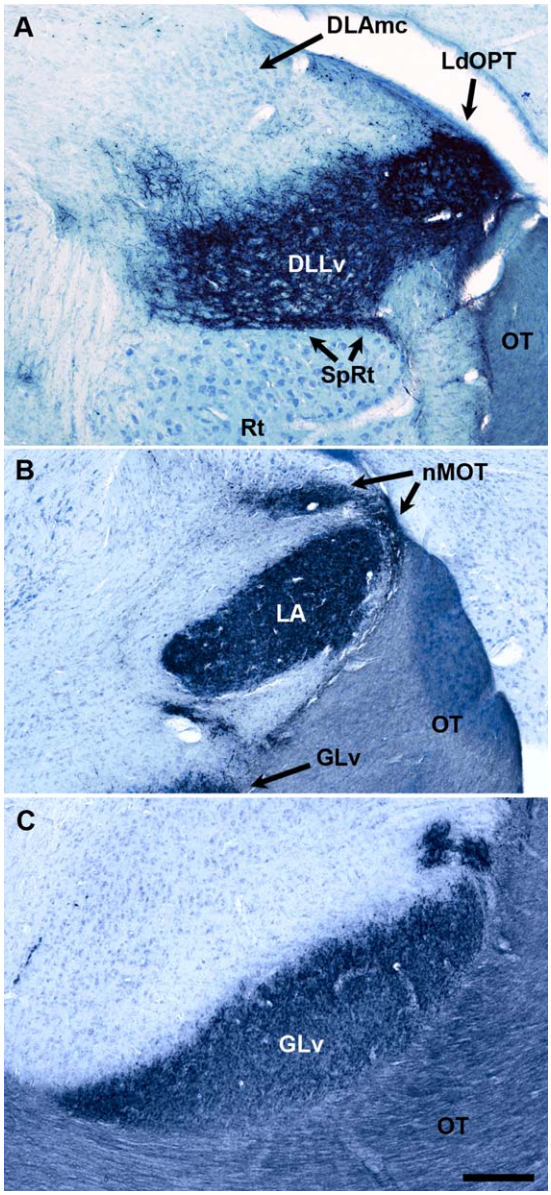

Figure 8. Detailed view of the retinal projection pattern to the contralateral thalamus. **A:** Photomicrographs of a coronal section through the anterior thalamus showing the retinorecipient substructures of the GLd complex. The strongest input is found in the DLLv, SpRt, and LdOPT, the latter appearing very distinct due to the strongly labeled dense terminals. The DLAmc receives very little or no retinal input. **B:** Terminal fields in the LA and the surrounding nMOT. **C:** Dense terminals in the lamina externa of the GLv in the ventral thalamus. Counterstained with Giemsa. For abbreviations, see list. Scale bar = 200 μm in C (applies to A–C). [Color figure can be viewed in the online issue, which is available at wileyonlinelibrary.com.]

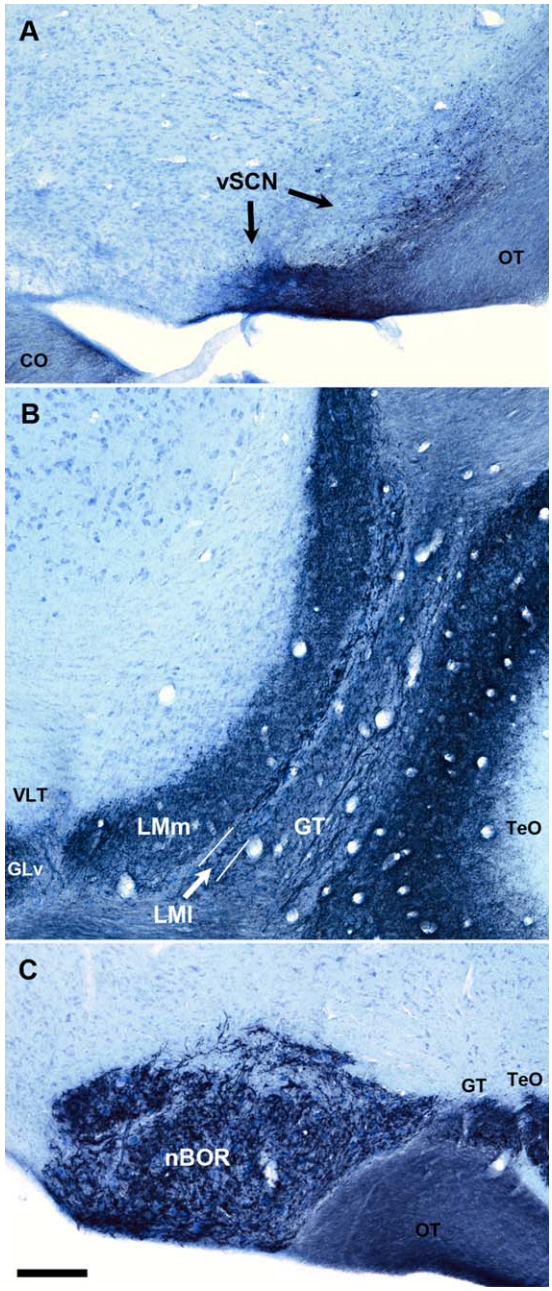

Figure 9. Detailed view of retinal projections to the hypothalamus, pretectum, and accessory optic system. **A:** Photomicrograph of a coronal section through the hypothalamus showing scattered terminal fields in the vSCN. **B:** In the pretectum, dense terminal fields are found in the GT and the two substructures of the LM (LMl and LMm). **C:** The GT continues toward the posterior until adjoining the nBOR. Counterstained with Giemsa. For abbreviations, see list. Scale bar = 200 μm in C (applies to A–C). [Color figure can be viewed in the online issue, which is available at wileyonlinelibrary.com.]

pretectalis (AP) and especially its dorsal subdivision, the *area pretectalis pars dorsalis* (APd), which was strongly labeled (Fig. 7F). In all these structures (the GT, LM, AP, and APd), very sparse ipsilateral retinal terminals were also found (data not shown). At the posterior margin of the optic tract, we found dense retinal terminals in the nucleus of the basal optic root (nBOR; Figs. 7F, 9C), which forms part of the accessory optic system

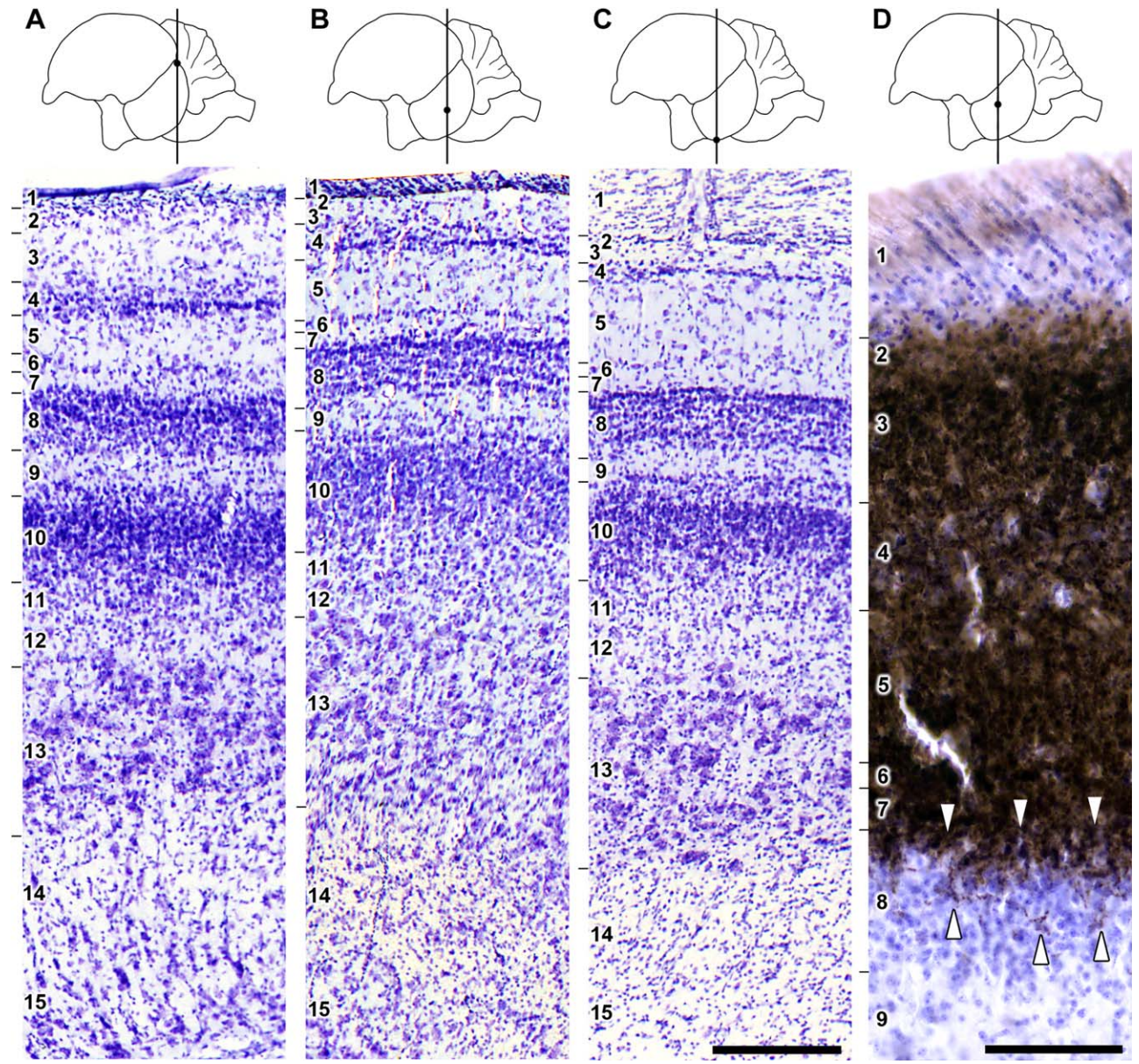

Figure 10. Morphology of the tectal layers. Lamination pattern in the dorsal (**A**), lateral (**B**), and ventral (**C**) TeO, and enlarged view of the CTB-reacted retinorecipient layers (**D**). Relative widths of tectal layers vary considerably from dorsal to ventral. The retinorecipient layer L5 increases from dorsal to ventral, whereas L2 and L3, and also L4, diminish. L6 and L7, in contrast, have a relatively constant width. Layer L8 is very conspicuous compared with other birds, not only because of its thickness, but most notably because it contains retinal terminals (arrowheads in D). All sections are stained with Nissl. Scale bar = 200 μm in C (applies to A–C); 100 μm in D. [Color figure can be viewed in the online issue, which is available at wileyonlinelibrary.com.]

(AOS). Sparse terminals were also found on the ipsilateral side (data not shown).

Optic tectum

The whole anteroposterior and dorsoventral extent of the TeO was labeled by anti-CTB immunohistochemistry (Fig. 6), showing that the intraocularly injected tracer had been taken up uniformly across the entire retina. All retinal projections were exclusive to the contralateral TeO. Dense terminals were found in the superficial layers (L2–L7) of the *stratum griseum et fibrosum superficiale* (SGFS). The layers that receive retinal afferents vary considerably in thickness along the dorsoventral axis of the TeO (Fig. 10). Whereas in the dorsal aspect, L3 and L4 cover more than half the width of all retinorecipient layers taken together, in the lateral aspect they cover little more than a third and in the ventral aspect less than a third. By contrast, L5 gains in width

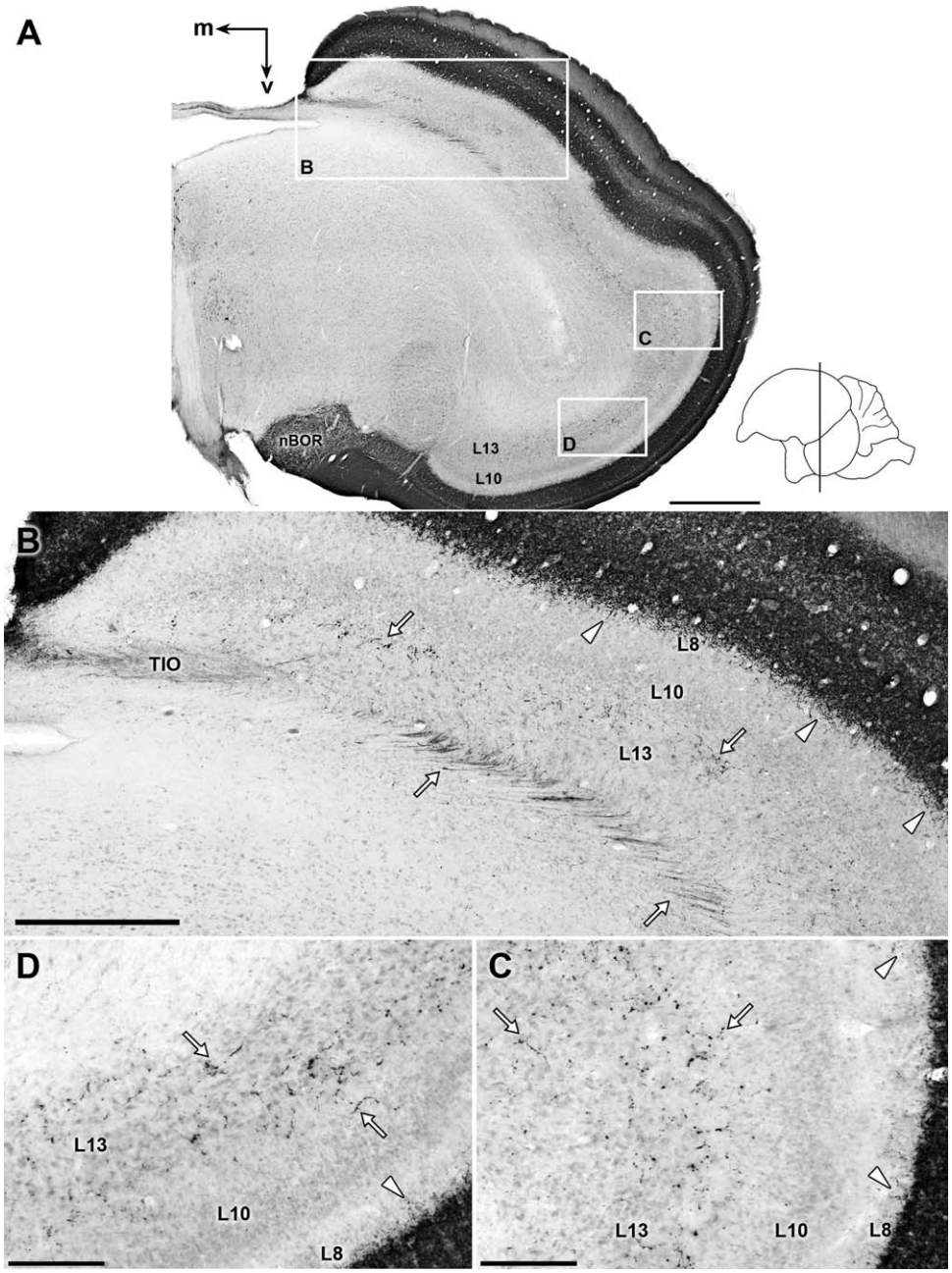

Figure 11. Deep tectal terminals after intraocular CTB injection. **A:** Overview of a coronal section through the contralateral TeO, with the indication of subsequent insets (BD). **B:** Origin of the deep pathway and terminals in L11–13. A fiber tract enters the TeO laterally (left arrow), branching off from the isthmo-optic tract (TIO). The fibers run along the periventricular zone (upward arrows) and turn radially outward to reach their target areas (downward arrows). Note also that retinal terminals exceeding the classical retinorecipient layers 1–7 and entering L8 can be distinguished (arrowheads; compare Fig. 10). **C,D:** Detailed photomicrographs of deep tectal varicosities (arrows) in the dorsal (B), lateral (C), and ventral (D) parts of the TeO, demonstrating their ubiquity. As in B, retinal terminals in L8 are very conspicuous (arrowheads). Counterstained with Giemsa. Scale bar = 1 mm in A; 500 μm in B; 200 μm in C,D.

from dorsal to ventral, occupying little over a quarter of the total thickness dorsally, to almost a half laterally and more than a half ventrally. Layers L2, L6, and L7 do not change notably in width, although L6 contains a substantially lower density of neurons in the ventral aspect than in the lateral and dorsal aspects.

In addition to the classical tectal retinorecipient layers 1–7, a considerable amount of retinal terminals surpassed L7 and entered L8 (Figs. 10, 11). Here they formed sparse ramifications, mostly in the outer two-thirds of the lamina, but sometimes throughout its extent. L9 did not contain any terminals or fibers.

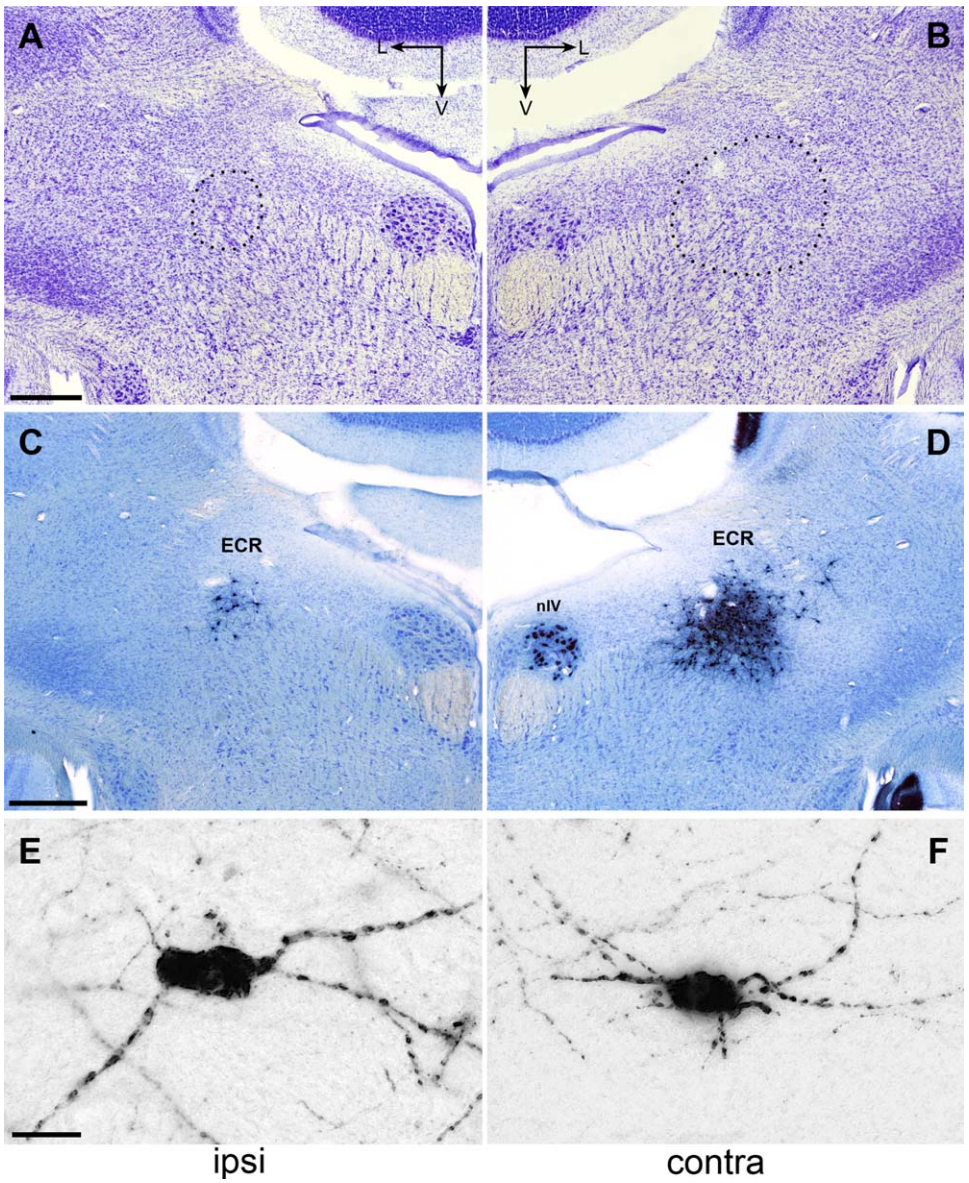

Figure 12. The isthmo-optic region of the Chilean tinamou, demonstrated by an intraocular CTB-injection. Coronal sections through the isthmic region ipsilateral (A,C E) and contralateral (B,D,F) to the injected eye. Note that although no structured isthmo-optic nucleus (ION) is distinguishable in Nissl-stained sections (**A,B**), anti-CTB reaction reveals a large number of contralateral, and a lower number of ipsilateral, retrogradely labeled centrifugal neurons (**C,D**). The great majority of these neurons are large (>20 μm) and multipolar (**E,F**), resembling the ectopic cells surrounding the ION of Neognathous birds. A and C as well as B and D, respectively, are consecutive sections from two series of the same brain, thus representing almost identical positions. Orientations given in A and B apply for all panels of their respective columns. On the contralateral side, the oculomotor nucleus trochlearis (nIV) also contains some retrogradely labeled neurons (see D), presumably from tracer spill into the periocular space. C and D are counterstained with Giemsa. E and F are extended focal imaging (EFI) extractions of z-stacks. ECR, ectopic cell region. Scale bar 500 μm in A (applies to A,B) and C (applies to C,D); 20 μm in E (applies to E,F). [Color figure can be viewed in the online issue, which is available at wileyonlinelibrary.com.]

Notably, in all intraocular injections, we found a sparse but evident amount of fibers and terminals forming a conspicuous band from layers L11 through L13 (Fig. 11). The density and distribution of these deep tectal terminals was fairly uniform across the entire TeO from anterior to posterior, but was more concentrated in the dorsal than in the ventral TeO (Fig. 11B–D). These "deep terminals" do not correspond to retinal fibers coursing radially from layer 7 toward the deep tectal layers. Instead, they represent terminals of axons that branch off

TABLE 1.
Primary Antibody Used in This Study

Antigen	Immunogen	Details	Dilution
CTB (cholera toxin subunit B)	Purified choleragenoid (cholera toxin subunit B aggregate)	List Biological, goat polyclonal, cat. no. 703, RRID:AB_10013220	1:40,000

from the isthmo-optic tract (TIO; Fig. 11A,B) and then proceed laterally into the TeO, running along L15 and the tectal ventricle. Thereafter, they bend off to cross radially through layers L14 and L13 toward their terminal location (Fig. 11A,B). The terminals have a striking morphology, with large bulbous-like varicosities that are distributed in layers L11 and L12, and more densely in L13 (Fig. 11C,D). L10 is almost completely free of such terminals.

Centrifugal neurons (ION)

In the dorsocaudal isthmus of the midbrain, a large quantity of retrogradely labeled neurons was found on the contralateral side (Fig. 12D), and a minor quantity on the ipsilateral side (Fig. 12C). These retinopetal (centrifugal) neurons were scattered over a considerable area within the neuroanatomical region of the avian isthmo-optic nucleus (ION) and its ectopic cell region (ECR). However, in Nissl-stained sections a clear nuclear organization as observed in most birds was not recognizable (Fig. 12A,B; see also Gutiérrez-Ibáñez et al., 2012).

Our stereological estimation of the number of retrogradely labeled centrifugal neurons yielded 4,120 cells (CE = 0.0658) and 323 cells (CE = 0.0963) on the contralateral and the ipsilateral side, respectively. Mean diameters of contralateral profiles varied from 8.2 to 24.5 μm, with an average of 16.4 ± 3.1 μm. Those of ipsilateral profiles varied from 12.6 to 22.2 μm, with an average of 17.6 ± 2.7 μm. Note that the neurons' orientations could not be taken into account for the measurements. Morphologically, the neurons were mostly large and multipolar (Fig. 12E,F), whereas smaller monopolar and fusiform neurons resembling typical avian isthmo-optic neurons were scarce.

DISCUSSION

In this study, we provide the first results of a systematic investigation of the visual pathways of a Palaeognathae representative, the Chilean tinamou (*Nothoprocta perdicaria*). We show that the retina of the tinamou possesses an elevated number of ganglion cells arranged in three distinct topographical specializations: an area centralis (AC) with a shallow fovea, a horizontal visual streak, and a dorsotemporal area (DTA). Accordingly, the visual field is highly panoramic, with a restricted frontal binocular overlap. As can be seen in our neuronal tracer data, the normal avian pattern of retinal central projections is well-developed and differentiated. However, we also found a remarkable projection to the deep layers of the TeO labeled after intraocular CTB injection. Similar projections have previously been described in embryonic chickens but are absent in adult animals (Wizenmann and Thanos, 1990; Omi et al., 2011).

Although no clear ION (Repérant et al., 2006) is distinguishable (Fig. 12A,B; Gutiérrez-Ibáñez et al., 2012), we found a high number of retrogradely labeled centrifugal neurons in the dorsal isthmic region, some of them projecting to the ipsilateral retina (Fig. 12C–F). Because tinamous represent a "basal" avian group, their centrifugal visual system may represent the link between the well-defined ION of most neognathous birds and the centrifugal visual system of the closest living relatives to birds, crocodiles (Müller and Reisz, 2005), who like the Chilean tinamou, also show a diffuse arrangement of the isthmo-optic neurons (Médina et al., 2004).

Visual field

Visual field measurements can tell us a great deal about animals' ecology and behavior (Martin, 2007). The most interesting aspects are the size and position of the frontal binocular overlap, the general extent of the lateral monocular fields, and the size of the blind area behind the bird. With respect to the binocular field, Martin (2007) distinguishes three main types in birds: Type 1 fields, with a binocular overlap between 20° and 30°, the bill's projection falling centrally or slightly below the center, and with a blind area behind the head; type 2 fields with ≤10° overlap, the bill at its periphery or outside, and no blind area to the rear; and type 3 fields, with large overlaps and large blind areas behind (owls). According to this schematic, the Chilean tinamou barely has a type 1 field (Fig. 2), which is mostly found in birds that forage by visual guidance of the bill (e.g., pecking), and/or that care for their chicks by feeding them (Martin et al., 2005; Martin, 2007). Tinamous do forage by pecking and by using their bill to dig in the ground for food (Cabot, 1992). In comparison with the other Palaeognaths studied, the binocular field of the Chilean tinamou appears to be similar to that of

the ostrich (Martin and Katzir, 1995), and larger than that of the kiwi, which is a nocturnal bird with a specialized olfactory sense (Martin et al., 2007).

The binocular field of the Chilean tinamou is presumably rather restricted, but with the aid of convergent eye movements it could become larger and include the retinal DTAs (especially around the bill). This could provide increased spatial resolution, and perhaps stereopsis. It may also provide functions for optic flow-field integration, which seems to be an important function of binocularity in birds (Martin and Katzir, 1999; Martin, 2007).

RGC density and visual acuity

The Chilean tinamou shows a variety of traits and specializations, which indicate a strong reliance on its visual sense. The "eye shape" value of −0.232 is typical of a diurnal bird (Hall and Ross, 2007; Lisney et al., 2012a). In the retina, we found a high overall quantity of approximately 4.3 million neurons. We could not quantify the ratio of the displaced amacrine cell population included in our data, because a distinction by morphological criteria (Ehrlich, 1981) was not practicable in retinal areas of high neuron densities (Collin and Pettigrew, 1988; Lisney and Collin, 2008; Lisney et al., 2012b; Wathey and Pettigrew, 1989). In various neognathous birds, displaced amacrine cells have been reported to constitute varying portions of the GCL neurons, for instance 30–35% (Ehrlich, 1981) or 32% (Chen and Naito, 1999) in the chicken, 11% (Hayes, 1984) or 40% (Binggeli and Paule, 1969) in the pigeon, or 20–30% in the quail (Muchnick and Hibbard, 1980). Arguably, we could have applied one of those ratios to our data, but given the considerable variation among Neognathae, we did not see a benefit in doing so.

Despite this caveat, the overall GCL count found in the tinamou is high compared with similar counts estimated for many other birds, such as Galliformes (Budnik et al., 1984; Ehrlich, 1981; Ikushima et al., 1986; Lisney et al., 2012b), Anseriformes (Fernández-Juricic et al., 2011; Lisney et al., 2013; Rahman et al., 2007a), Columbiformes (Binggeli and Paule, 1969), Passeriformes (Coimbra et al., 2006, 2009; Rahman et al., 2006, 2007b), various Strigiformes (barn owl, northern saw-whet owl, short-eared owl; Lisney et al., 2012a; Wathey and Pettigrew, 1989), Procellariiformes (Hayes and Brooke, 1990), Sphenisciformes (Coimbra et al., 2012), and Struthioniformes (ostrich; Boire et al., 2001). Of all the avian species studied so far, the Chilean tinamou is only surpassed by some particularly visually-specialized ones, for instance some owls (snowy owl, great horned owl, great gray owl, barred owl, and northern hawk owl; Lisney et al., 2012a), probably kingfishers (Moroney and Pettigrew, 1987), and Falconiformes (Inzunza et al., 1991), although in the latter two cases no total RGC number quantifications have been provided by the authors.

With respect to the maximal GCL neuron density, the Chilean tinamou also ranks high among birds, if not vertebrates. In Neognathae, the displaced amacrine cell density is reportedly uniform across the entire retina (Ehrlich, 1981) and of a negligible magnitude for RGC estimations in high-density areas (Bravo and Pettigrew, 1981; Collin and Pettigrew, 1988). Therefore, our estimation of 61.9×10^3 neurons/mm^2 in the AC probably corresponds to true RGCs (see above), almost reaching the values obtained in eagles and hawks, who possess 65 and 62×10^3 cells/mm^2 in the foveal region of their GCL, respectively (Inzunza et al., 1991).

However, visual acuity is not only limited by the density of RGCs, but also by the eye's focal length, which is proportional to its axial length (Hall and Ross, 2007; Martin, 1993; Walls, 1942). The theoretical SRP can be estimated from the eye's focal length and the maximal RGC density under the assumption that one cycle of grating can be resolved by two adjacent ganglion cells (Collin and Pettigrew, 1989; Pettigrew et al., 1988; Ullmann et al., 2012). The Chilean tinamou's relatively high SRP value of 13.6–14.0 cycles/degree, higher than, for example, phasianid Galliformes such as the chicken (6.5–8.6 cycles/degree; Gover et al., 2009; Schmid and Wildsoet, 1998) or the quail (4.3–4.9 cycles/degree; Lee et al., 1997), reflects the relatively small eyes of this bird, for which the high RGC density can only partly compensate. In contrast, the ostrich, despite its relatively low maximal RGC density of approximately 9,000 cells/mm^2, has a high estimated SRP of between 17.0 and 22.5 cycles/degree (Boire et al., 2001) because of its large eyes (axial length 39 mm; Martin and Katzir, 1995). Thus, the high number and density of RGCs in the Chilean tinamou retina can be seen as a way to increase visual acuity within the anatomical constraint of a relatively small eye size.

Retinal topography

Topographical specializations in the retinal cell distribution have long been recognized to be of importance for eco-behavioral functioning of vertebrate vision (Hughes, 1977). Three distinct types of *areae* (AC, horizontal visual streak, and DTA) characterized by elevated retinal cell densities are frequently found in birds (Güntürkün, 2000), and all of them are present in the Chilean tinamou (Figs. 3, 4). The AC, which subserves the bird's lateral visual field, contains in addition to the already-discussed high RGC density a shallow concaviclivate fovea (Fig. 4A,B). This type of fovea, in contrast to the deep convexiclivate type (Walls, 1963), covers a wider retinal area and has

been proposed to accomplish a better functionality in vigilance behavior (Fernández-Juricic, 2012). In comparison, the most basal Neognathae and thus closest neognathous relatives, Galliformes, generally do not possess a fovea in their retina (Lisney et al., 2012b), although the quail has been reported to have a shallow one (Ikushima et al., 1986). It has to be noted, however, that the tinamou specimens used in this study were acquired from a breeder. Thus, the shallowness of the fovea could be the result of domestication, which has been reported to alter the fundus oculi considerably (Walls, 1942; Wood, 1917), and wild tinamous might possess a more pronounced fovea than described here.

Distinct from the AC, a large DTA covers almost a quadrant of the Chilean tinamou retina (Fig. 3). The presence of a DTA (or area dorsalis) is an often-found retinal feature of granivorous birds (Budnik et al., 1984; Güntürkün, 2000), because it covers the anteroventral aspect of the visual field and thus aids in object (food) recognition and pecking behavior (Martin, 2007; Nalbach et al., 1990). Fittingly, the Chilean tinamou's diet, which consists mostly of seeds and sometimes insects, is gathered by pecking and digging with the beak (Cabot, 1992; Conover, 1924). Interestingly, in contrast to this idea, a number of phasianid Galliformes reportedly lack a DTA, even though they are ground-foragers (Lisney et al., 2012b). Thus, other factors may contribute to the presence or absence of a DTA in a bird species, and it is definitely curious that the basal tinamou possesses this feature whereas many Galliformes do not.

Engulfing the AC, but distinct from the DTA, the tinamou retina also features a horizontal visual streak (Fig. 3). According to the *Terrain Hypothesis* (Hughes, 1977), this specialization frequently evolves in animals living in open or semi-open habitats without dense arboreal vegetation, because it provides them with improved visual capacities for scanning the horizon, e.g., for predators. Quite a number of studies support this proposition, such as in the red kangaroo *Macropus rufus* (Hughes, 1975), the giraffe *Giraffa camelopardalis* (Coimbra et al., 2013), anatid ducks (Lisney et al., 2013), the Canada goose *Branta canadensis* (Fernández-Juricic et al., 2011), seabirds (Hayes and Brooke, 1990), and non-nocturnal owls living in open habitats (Lisney et al., 2012a), and even in such distant species as nonvertebrate crabs (Zeil et al., 1986) or coleoid cephalopods (Talbot and Marshall, 2011). Also, another palaeognathous bird species, the ostrich *Struthio camelus* (Boire et al., 2001), which lives in the savannas and Sahel of Africa, possesses a pronounced horizontal visual streak. The Chilean tinamou conforms well to this hypothesis, because it lives exclusively in open habitats (Cabot, 1992; Conover, 1924).

Central retinal projections

The overall pattern of retinal projections in the Chilean tinamou is mostly consistent with the pattern found in Neognathous birds, implying that this shared organization of the avian visual system was fully present in the last common ancestors of Palaeognathae and Neognathae over 120 million years ago, and has in both groups remained highly conserved during this long time span of separate evolution.

Dorsal thalamus

Representing the first stage of the thalamofugal pathway, the dorsal lateral geniculate (GLd) of the tinamou receives considerable input (Figs. 7C,D, 8A), although clearly not as much as the TeO. Similar to the pigeon (Güntürkün and Karten, 1991; Güntürkün et al., 1993; Miceli et al., 1975, 2008) and the quail (Watanabe, 1987), the strongest retinorecipient GLd elements are the ventral portion of the DLL (= DLLv of Miceli et al., 2008), its most ventral subdivision, the SpRt, and the LdOPT (we adhere to the nomenclature of Güntürkün and Karten, 1991, whereas others have identified it as the DLAlr [Ehrlich and Mark, 1984a; Watanabe, 1987], or as a portion of the DLLd [Miceli et al., 1975, 2008]). The high density and defined pattern of retinal input in the LdOPT suggest that it is an important relay of the tinamou's thalamofugal pathway, similar to what is assumed in neognathous birds (Ehrlich and Mark, 1984a; Watanabe, 1987). In addition, it contains conspicuously large retinal terminals (Fig. 8A), analogous to what has been noted in the pigeon (Güntürkün and Karten, 1991).

Ventral thalamus

The ventral thalamus of the tinamou appears to be very similar compared with other birds. The LA and GLv are well developed (Figs. 7A–E, 8B,C), and the GLv-ne of the latter is densely innervated by retinal terminals. The nMOT (Figs. 7B–D, 8B), which may be the homologue of the mammalian intergeniculate leaflet (IGL; Güntürkün and Karten, 1991; Harrington, 1997), has rather scarce retinal innervation compared with the pigeon (Güntürkün and Karten, 1991); however, its general neuroanatomical organization is very similar.

Hypothalamus

Retinal input to the avian hypothalamus is mainly confined to a small lateral portion (Cantwell and Cassone, 2006; Cassone and Moore, 1987; Cooper et al., 1983; Gamlin et al., 1982; Norgren and Silver, 1989b; Shimizu et al., 1994). Some studies also report scarce retinal afferents to a second, medial hypothalamic division, e.g., in the pigeon (Shimizu et al., 1994) and in the chicken (Cantwell

and Cassone, 2006). In the palaeognathous tinamou we could not find any retinal terminals or fibers in the medial hypothalamic region; however, we found input to the lateral portion (Figs. 7A, 9A), which we call the vSCN, following the nomenclature of Cantwell and Cassone (2006). Interestingly, in the closest extant relatives of birds, the crocodiles, retinohypothalamic projections to both a lateral and a medial portion of the hypothalamus have been described (Derobert et al., 1999).

Pretectum and AOS

We generally found the typical avian retinal projection pattern to the pretectum and AOS (Figs. 7D–F, 9B,C) that, for example, has been described in the chicken (Ehrlich and Mark, 1984a), the quail (Norgren and Silver, 1989a), and the pigeon (Gamlin and Cohen, 1988a). On the contralateral side, the projections comprise a large and densely labeled GT, LMm, and LMl, as well as a substantial nBOR of the AOS. Furthermore, the AP and especially its dorsal subdivision (APd) were labeled from retinal input, similar to the description by Gamlin and Cohen (1988a) and Shimizu et al. (1994) in the pigeon.

Optic tectum

The tinamou's TeO, which in birds generally receives the majority of retinal fibers (Benowitz and Karten, 1976; Luksch, 2003; Mpodozis et al., 1995; Ramón y Cajal, 1909; Wylie et al., 2009), is particularly prominent (Fig. 6). Its retinorecipient layers 1–7 receive dense afferents (Fig. 10D), suggesting a tectofugal pathway of considerable proportions. The dominance of the tectofugal pathway appears to be a common trait in Tinamiformes, because two other species of this family are reported to possess large tectofugal components relative to brain volume (Bee de Speroni and Carezzano, 1995; Iwaniuk et al., 2010).

The general organization of the Chilean tinamou TeO is similar to that of neognathous birds. Altogether, its lamination appears to be more complex than in the chicken TeO (Karten, 2007), but not as complex as a passerine TeO (Faunes et al., 2013; Karten et al., 2013). The relative width changes of the various tectal layers from dorsal to ventral (especially L5; see Results; Fig. 10) are generally similar to findings in the pigeon (Karten et al., 1997). In the pigeon, however, the change in L5 is more dramatic (compare Fig. 6 of Karten et al., 1997) and whereas in the pigeon L4 is almost nonexistent in the ventral TeO, in the tinamou it remains a thin but distinct lamina (Fig. 10C).

We found that layer 8 is relatively prominent in the tinamou, and, interestingly, although classically considered non-retinorecipient, it receives retinal terminals throughout the TeO (Fig. 10D; arrowheads in Fig. 11). To our knowledge, this has not been reported in an adult bird. However, an even denser L8 projection appears to be present in a neognathous Caprimulgiform, the band-winged nightjar *Caprimulgus (Systellura) longirostris* (Juan E. Salazar and Jorge Mpodozis, manuscript in preparation, personal communication). It has been shown in chicken that during embryonic development, retinal fibers pervade the classical retinorecipient layers 1–7 and intrude into L8 and L9; a few even intrude into L10. This transient projection progresses until E14, begins to degenerate at E16, and is almost gone by E17 (Omi et al., 2011). Possibly, this embryonic projection is maintained in some birds such as the Chilean tinamou and the band-winged nightjar. Because both birds possess an enlarged L8, this retinal projection may have to do with a functional specialization of this lamina.

We regard the finding of fibers and terminals in the deep tectal layers 11–13 (Fig. 11) as a very significant result. Because they were labeled by intraocular tracer injections, they either represent a projection from retinal neurons or collateral branches from ION neurons projecting to the retina.

In embryonic chickens, a very similar pathway has been described by Omi et al. (2011), which first appears at E8–E9, degenerates from E14 onward, and entirely disappears after hatching. These authors assumed that this projection originated in the retina, stating that the "retinal fibers. . .run [dorsally] along the medial edge of the TeO after invading the tectum and turn toward the lateral side." The fibers that seem to give rise to the deep tectal terminals in the tinamou fit rather well with this description in that they seem to enter the tectum at its dorsomedial margin and then turn laterally. However, when these fiber bundles are followed along the transverse section series from anterior to posterior, they surprisingly form a continuum with the TIO (Fig. 11B; compare Fig. 7F). Thus, they may be either retinal fibers running along the TIO, or they may even be bifurcating side branches of the TIO providing a feedback from the centrifugal system to the TeO. In fact, Wizenmann and Thanos (1990) traced a transient projection from centrifugal ION neurons to the tectum between E9 and E16, which was corroborated by double-labeling experiments. It is therefore probable that the results reported by Omi et al. (2011) represent the same transient projection from the ION to the TeO, rather than a retinal projection. At present, we cannot decide between either possibilities and further experiments will be needed to clarify the source of these terminals. Whatever the case, the deep tectal pathway of the adult tinamou would be equivalent to pathways transiently expressed in Neognaths such as the chicken.

Centrifugal visual system

The centrifugal visual system of birds generally consists of two components, the organized ION and a surrounding region of "ectopic cells" (EC) (Clarke and Cowan, 1975; Hayes and Webster, 1981; Miceli et al., 1999; Wilson and Lindstrom, 2011), both respectively projecting to the retina in a characteristic fashion (Nickla et al., 1994; Uchiyama et al., 2004). Although most birds examined to date possess a well-defined ION, a recent large-scale comparative study in which the authors examined Nissl material of several dozen bird species could not find any distinguishable ION in the Chilean tinamou (Gutiérrez-Ibáñez et al., 2012). Similarly, two other palaeognathous birds were previously reported to lack an ION—the brown kiwi (Craigie, 1930) and the ostrich (Verhaart, 1971).

Retrograde labeling from our intraocular tracer experiments has now revealed that the Chilean tinamou possesses a considerable population of centrifugal neurons (Fig. 12). These cells appear to correspond mostly to ECs, for several reasons: First, they are not organized in a distinctive nuclear structure as is the typical neognathous ION. Second, we were unable to identify tufted monopolar neurons resembling "true" ION neurons of Neognathae (Cowan, 1970; Miceli et al., 1995). Instead, all of the tinamou's centrifugal neurons appear to be large and multipolar (Fig. 12E,F), like the ECs of neognathous birds (Cowan and Clarke, 1976). Third, a portion of the cells project to the ipsilateral retina (Fig. 12C,E), a common characteristic of avian ECs (Repérant et al., 2006).

Intriguingly, the tinamou isthmo-optic system bears a striking resemblance to the centrifugal visual system of crocodilians, the closest extant relatives of birds (Müller and Reisz, 2005). The homology of the centrifugal visual system in the Archosauria is stressed by the finding that the large majority of centrifugal neurons of both *Crocodylus niloticus* (Médina et al., 2004) and *Caiman crocodilus* (Ferguson et al., 1978) reside in an isthmic region with the same embryological origin as the avian isthmo-optic system (rhombomere 0) (Clarke and Cowan, 1976; Cowan and Clarke, 1976; Médina et al., 2004; O'Leary and Cowan, 1982; Repérant et al., 2007).

Like avian ECs (and tinamou isthmo-optic neurons), the crocodilian isthmo-optic system does not possess any clearly organized nuclear structure (Médina et al., 2004). In addition, morphologically the crocodilian centrifugal neurons closely resemble the ECs of birds, because in both the crocodile and the caiman most of these neurons are multipolar or fusiform. Although the existence of a few monopolar neurons resembling neognathous ION cells was reported in the crocodile, they do not project exclusively to the contralateral retina like neognathous "true" ION cells (Médina et al., 2004), and furthermore, the caiman completely lacks such cells (Ferguson et al., 1978).

Therefore, it is possible that the "true" isthmo-optic nucleus is a synapomorphy of Neognathae, and some characteristics of the basal "crocodilian" condition (e.g., only "ectopic" centrifugal neurons) are maintained in palaeognathous birds. The alternative possibility would be that a "true" ION was present in the last common ancestor of Palaeognathae and Neognathae, but was secondarily reduced in the tinamou. In fact, this may have occurred in some nonbasal neognathous species of the order Procellariiformes and the closely related pelicans (Gutiérrez-Ibáñez et al., 2012). Unfortunately, no retrograde tracing studies have been conducted in these species, so the existence of a perhaps small but "true" ION cannot be ruled out. A well-organized ION is such a widespread condition in Neognathae that it seems likely that a palaeognathous centrifugal visual system composed of ectopic cells as in the tinamou is indeed an ancestral condition and unique among birds. On the grounds of these points, the centrifugal visual system of Palaeognathae such as the Chilean tinamou may represent an intermediate stage between crocodiles and neognathous birds, filling a gap of approximately 250 million years since the crocodile-bird split (Müller and Reisz, 2005).

CONCLUSIONS: WHY STUDY TINAMOUS?

The present study provides for the first time a comprehensive description of the visual system of a palaeognathous bird, including its visual field, retinal topography, and retinal connections. Although it is clear that in general the visual system is highly conserved across the Amniote phylum, the comparative study of a basal bird may help to elucidate important aspects of its evolution in finer detail. Because of the long evolutionary divergence between the Neognathae and Palaeognathae, both similarities and differences between these clades are of interest. The similarities (conserved characteristics) may represent the basal avian conditions that existed in their common ancestors over 120 million years ago, whereas the differences illustrate which elements of the avian visual system have been subjected to evolutionary change.

At the level of retino-central connectivity of the tinamou, two elements have emerged as interesting differences to Neognathae and deserve further investigation: First, the adult deep tectal terminals, which in Neognathae have only been reported at embryonic stages; and second, the centrifugal visual system, which appears to resemble more closely the crocodilian than the neognathous avian condition.

Future research should also investigate the tinamou's higher visual projections, as well as the central organization of other sensory pathways. Qualitative observations of Nissl-stained material (as is shown in Fig. 6) reveal interesting cytoarchitectonics in field L, the n. basalis, the arcopallium, and the Wulst. A better understanding of the tinamou's pallial circuits would contribute to widening the basis for comparative studies across vertebrates, providing new insights about the evolution of the pallium and of the brain organization as a whole.

ACKNOWLEDGMENTS

We thank Birgit Seibel, Yvonne Schwarz, Gaby Schwabedissen, Elisa Sentis, and Solano Henriquez for excellent technical assistance. Thanks also to Dr. Jorge Mpodozis, Dr. Cristián Gutiérrez-Ibáñez, Dr. Michael Gebhardt and Juan E. Salazar for providing helpful comments during the conduct of this research and for valuable feedback on the manuscript. Thanks furthermore to Jared D. Lockwood for his linguistic comments. We are grateful to Sergio Bitran M. for permitting us to use his photography of a wild Chilean tinamou in this paper.

CONFLICT OF INTEREST STATEMENT

The authors declare they have no conflicts of interest.

ROLE OF AUTHORS

All authors had full access to all the data in the study and take responsibility for the integrity of the data and the accuracy of the data analysis. Study concept and design: QK, GM, HL, TVZ. Acquisition of data: QK, CM, GM. Analysis and interpretation of data: QK, HL, TVZ, GM. Drafting of the manuscript: QK, GM, TVZ. Critical revision of the manuscript for important intellectual content: HL, GM, TVZ. Statistical analysis: QK. Obtained funding: GM, HL. Study supervision: HL and GM.

LITERATURE CITED

Bee de Speroni N, Carezzano F. 1995. Volumetric analysis of the visual, trigeminal and acoustic nuclei in four avian species (Rheidae, Spheniscidae, Tinamidae). Mar Ornith 23:11–15.

Benowitz LI, Karten HJ. 1976. Organization of the tectofugal visual pathway in the pigeon: a retrograde transport study. J Comp Neurol 167:503–520.

Bertelli S, Porzecanski AL. 2004. Tinamou (Tinamidae) systematics: a preliminary combined analysis of morphology and molecules. Ornitol Neotrop 15(suppl):1–7.

Bertelli S, Chiappe LM, Mayr G. 2014. Phylogenetic interrelationships of living and extinct Tinamidae, volant palaeognathous birds from the New World. Zool J Linnean Soc 172:145–184.

Binggeli RL, Paule WJ. 1969. The pigeon retina: quantitative aspects of the optic nerve and ganglion cell layer. J Comp Neurol 137:1–18.

Bischof H-J. 1988. The visual field and visually guided behavior in the zebra finch (*Taeniopygia guttata*). J Comp Physiol A 163:329–337.

Boire D, Dufour JS, Théoret H, Ptito M. 2001. Quantitative analysis of the retinal ganglion cell layer in the ostrich, *Struthio camelus*. Brain Behav Evol 58:343–355.

Bravo H, Pettigrew JD. 1981. The distribution of neurons projecting from the retina and visual cortex to the thalamus and tectum opticum of the barn owl, *Tyto alba*, and the burrowing owl, *Speotyto cunicularia*. J Comp Neurol 199: 419–441.

Brown J, Rest J, García-Moreno J, Sorenson M, Mindell D. 2008. Strong mitochondrial DNA support for a Cretaceous origin of modern avian lineages. BMC Biol 6:6.

Budnik V, Mpodozis J, Varela FJ, Maturana HR. 1984. Regional specialization of the quail retina: ganglion cell density and oil droplet distribution. Neurosci Lett 51:145–150.

Cabot J. 1992. Family Tinamidae (Tinamous). In: Del Hoyo J, Elliott A, Sargatal J (eds.). Handbook of the birds of the world. Vol. 1: Ostrich to ducks. Lynx Edicions, Barcelona, Spain, pp. 112–138.

Cantwell EL, Cassone VM. 2006. Chicken suprachiasmatic nuclei: I. Efferent and afferent connections. J Comp Neurol 496:97–120.

Carlo CN, Stevens CF. 2011. Analysis of differential shrinkage in frozen brain sections and its implications for the use of guard zones in stereology. J Comp Neurol 519:2803–2810.

Cassone VM, Moore RY. 1987. Retinohypothalamic projection and suprachiasmatic nucleus of the house sparrow, *Passer domesticus*. J Comp Neurol 266:171–182.

Chen Y, Naito J. 1999. A quantitative analysis of cells in the ganglion cell layer of the chick retina. Brain Behav Evol 53:75–86.

Clarke PGH, Cowan WM. 1975. Ectopic neurons and aberrant connections during neural development. Proc Natl Acad Sci U S A 72:4455–4458.

Clarke PGH, Cowan WM. 1976. The development of the isthmo-optic tract in the chick, with special reference to the occurrence and correction of developmental errors in the location and connections of isthmo-optic neurons. J Comp Neurol 167:143–163.

Coimbra JP, Marceliano MLV, Andrade-da-Costa BL da S, Yamada ES. 2006. The retina of tyrant flycatchers: topographic organization of neuronal density and size in the ganglion cell layer of the great kiskadee *Pitangus sulphuratus* and the rusty margined flycatcher *Myiozetetes cayanensis* (Aves: Tyrannidae). Brain Behav Evol 68:15–25.

Coimbra JP, Trévia N, Videira Marceliano ML, da Silveira Andrade-Da-Costa BL, Picanço-Diniz CW, Yamada ES. 2009. Number and distribution of neurons in the retinal ganglion cell layer in relation to foraging behaviors of tyrant flycatchers. J Comp Neurol 514:66–73.

Coimbra JP, Nolan PM, Collin SP, Hart NS. 2012. Retinal ganglion cell topography and spatial resolving power in penguins. Brain Behav Evol 80:254–268.

Coimbra JP, Hart NS, Collin SP, Manger PR. 2013. Scene from above: retinal ganglion cell topography and spatial resolving power in the giraffe (*Giraffa camelopardalis*). J Comp Neurol 521:2042–2057.

Collin SP, Pettigrew JD. 1988. Retinal ganglion cell topography in teleosts: a comparison between Nissl-stained material and retrograde labelling from the optic nerve. J Comp Neurol 276:412–422.

Collin SP, Pettigrew JD. 1989. Quantitative comparison of the limits on visual spatial resolution set by the ganglion cell

layer in twelve species of reef teleosts. Brain Behav Evol 34: 184–192.
Conover HB. 1924. A new subspecies of *Nothoprocta* from Chile. Auk 41:334–336.
Cooper ML, Pickard GE, Silver R. 1983. Retinohypothalamic pathway in the dove demonstrated by anterograde HRP. Brain Res Bull 10:715–718.
Corfield JR, Wild JM, Hauber ME, Parsons S, Kubke MF. 2008. Evolution of brain size in the Palaeognath lineage, with an emphasis on new zealand ratites. Brain Behav Evol 71:87–99.
Corfield JR, Wild JM, Parsons S, Kubke MF. 2012. Morphometric analysis of telencephalic structure in a variety of Neognath and Paleognath bird species reveals regional differences associated with specific behavioral traits. Brain Behav Evol 80:181–195.
Cowan WM. 1970. Centrifugal fibres to the avian retina. Br Med Bull 26:112–118.
Cowan W, Clarke P. 1976. The development of the isthmo-optic nucleus. Brain Behav Evol 13:345–375.
Craigie EH. 1930. Studies on the brain of the kiwi (*Apteryx australis*). J Comp Neurol 49:223–357.
Derobert Y, Médina M, Rio J-P, Ward R, Repérant J, Marchand M-J, Miceli D. 1999. Retinal projections in two crocodilian species, *Caiman crocodilus* and *Crocodylus niloticus*. Anat Embryol 200:175–191.
Ehrlich D. 1981. Regional specialization of the chick retina as revealed by the size and density of neurons in the ganglion cell layer. J Comp Neurol 195:643–657.
Ehrlich D, Mark R. 1984a. An atlas of the primary visual projections in the brain of the chick *Gallus gallus*. J Comp Neurol 223:592–610.
Ehrlich D, Mark R. 1984b. Topography of primary visual centres in the brain of the chick, *Gallus gallus*. J Comp Neurol 223:611–625.
Faunes M, Fernández S, Gutiérrez-Ibáñez C, Iwaniuk AN, Wylie DR, Mpodozis J, Karten HJ, Marín G. 2013. Laminar segregation of GABAergic neurons in the avian nucleus isthmi pars magnocellularis: a retrograde tracer and comparative study. J Comp Neurol 521:1727–1742.
Ferguson JL, Mulvanny PJ, Brauth SE. 1978. Distribution of neurons projecting to the retina of *Caiman crocodilus*. Brain Behav Evol 15:294–306.
Fernández-Juricic E. 2012. Sensory basis of vigilance behavior in birds: synthesis and future prospects. Behav Proc 89: 143–152.
Fernández-Juricic E, Moore BA, Doppler M, Freeman J, Blackwell BF, Lima SL, DeVault TL. 2011. Testing the terrain hypothesis: Canada geese see their world laterally and obliquely. Brain Behav Evol 77:147–158.
Gamlin PDR, Cohen DH. 1988a. Retinal projections to the pretectum in the pigeon (*Columba livia*). J Comp Neurol 269:1–17.
Gamlin PDR, Cohen DH. 1988b. Projections of the retinorecipient pretectal nuclei in the pigeon (*Columba livia*). J Comp Neurol 269:18–46.
Gamlin PD, Reiner A, Karten HJ. 1982. Substance P-containing neurons of the avian suprachiasmatic nucleus project directly to the nucleus of Edinger-Westphal. Proc Natl Acad Sci U S A 79:3891–3895.
Gover N, Jarvis JR, Abeyesinghe SM, Wathes CM. 2009. Stimulus luminance and the spatial acuity of domestic fowl (*Gallus g*. domesticus). Vision Res 49:2747–2753.
Green MA, Sviland L, Malcolm AJ, Pearson AD. 1989. Improved method for immunoperoxidase detection of membrane antigens in frozen sections. J Clin Pathol 42:875–880.
Guiloff GD, Maturana HR, Varela FJ. 1987. Cytoarchitecture of the avian ventral lateral geniculate nucleus. J Comp Neurol 264:509–526.
Gundersen HJG. 1977. Notes on the estimation of the numerical density of arbitrary profiles: the edge effect. J Microsc 111:219–223.
Gundersen HJG, Bagger P, Bendtsen TF, Evans SM, Korbo L, Marcussen N, Møller A, Nielsen K, Nyengaard JR, Pakkenberg B, Sørensen FB, Vesterby A, West MJ. 1988a. The new stereological tools: disector, fractionator, nucleator and point sampled intercepts and their use in pathological research and diagnosis. APMIS 96:857–881.
Gundersen HJG, Bendtsen TF, Korbo L, Marcussen N, Møller A, Nielsen K, Nyengaard JR, Pakkenberg B, Sørensen FB, Vesterby A, West MJ. 1988b. Some new, simple and efficient stereological methods and their use in pathological research and diagnosis. APMIS 96: 379–394.
Güntürkün O. 2000. Sensory physiology: vision. In: Sturkie PD, Whittow GC (eds.). Sturkie's avian physiology, 5th ed. New York, NY: Academic Press, pp. 1–19.
Güntürkün O, Karten HJ. 1991. An immunocytochemical analysis of the lateral geniculate complex in the pigeon (*Columba livia*). J Comp Neurol 314:721–749.
Güntürkün O, Miceli D, Watanabe M. 1993. Anatomy of the avian thalamofugal pathway. In: Zeigler HP, Bischof H-J (eds.). Vision, brain, and behavior in birds. Cambridge, MA: MIT Press, pp. 115–135.
Gutfreund Y. 2012. Stimulus-specific adaptation, habituation and change detection in the gaze control system. Biol Cybern 106:657–668.
Gutfreund Y, Zheng W, Knudsen EI. 2002. Gated visual input to the central auditory system. Science 297:1556–1559.
Gutiérrez-Ibáñez C, Iwaniuk AN, Lisney TJ, Faunes M, Marín GJ, Wylie DR. 2012. Functional implications of species differences in the size and morphology of the isthmo optic nucleus (ION) in birds. PLoS ONE 7:e37816.
Hackett SJ, Kimball RT, Reddy S, Bowie RCK, Braun EL, Braun MJ, Chojnowski JL, Cox WA, Han K-L, Harshman J, Huddleston CJ, Marks BD, Miglia KJ, Moore WS, Sheldon FH, Steadman DW, Witt CC, Yuri T. 2008. A Phylogenomic study of birds reveals their evolutionary history. Science 320:1763–1768.
Haddrath O, Baker AJ. 2012. Multiple nuclear genes and retroposons support vicariance and dispersal of the palaeognaths, and an Early Cretaceous origin of modern birds. Proc R Soc B Biol Sci 279:4617–4625.
Hall MI, Ross CF. 2007. Eye shape and activity pattern in birds. J Zool 271:437–444.
Harmening WM, Wagner H. 2011. From optics to attention: visual perception in barn owls. J Comp Physiol A 197: 1031–1042.
Harrington ME. 1997. The ventral lateral geniculate nucleus and the intergeniculate leaflet: interrelated structures in the visual and circadian systems. Neurosci Biobehav Rev 21:705–727.
Harshman J, Braun EL, Braun MJ, Huddleston CJ, Bowie RCK, Chojnowski JL, Hackett SJ, Han K-L, Kimball RT, Marks BD, Miglia KJ, Moore WS, Reddy S, Sheldon FH, Steadman DW, Steppan SJ, Witt CC, Yuri T. 2008. Phylogenomic evidence for multiple losses of flight in ratite birds. Proc Natl Acad Sci U S A 105:13462 –13467.
Hatton WJ, Von Bartheld CS. 1999. Analysis of cell death in the trochlear nucleus of the chick embryo: calibration of the optical disector counting method reveals systematic bias. J Comp Neurol 409:169–186.
Hayes BP. 1984. Cell populations of the ganglion cell layer: displaced amacrine and matching amacrine cells in the pigeon retina. Exp Brain Res 56:565–573.
Hayes BP, Brooke MDL. 1990. Retinal ganglion cell distribution and behaviour in procellariiform seabirds. Vision Res 30:1277–1289.

Hayes BP, Holden AL. 1983. The distribution of displaced ganglion cells in the retina of the pigeon. Exp Brain Res 49:181–188.

Hayes BP, Webster KE. 1981. Neurones situated outside the isthmo-optic nucleus and projecting to the eye in adult birds. Neurosci Lett 26:107–112.

Hughes A. 1975. A comparison of retinal ganglion cell topography in the plains and tree kangaroo. J Physiol (Lond) 244:61P–63P.

Hughes A. 1977. The topography of vision in mammals of contrasting life style: comparative optics and retinal organization. In: Crescitelli F (ed.). The visual system in vertebrates. Handbook of sensory physiology. New York, NY: Springer, pp. 613–756.

Ikushima M, Watanabe M, Ito H. 1986. Distribution and morphology of retinal ganglion cells in the Japanese quail. Brain Res 376:320–334.

Inzunza O, Bravo H, Smith RL, Angel M. 1991. Topography and morphology of retinal ganglion cells in Falconiforms: a study on predatory and carrion-eating birds. Anat Rec 229:271–277.

Iwaniuk AN, Dean KM, Nelson JE. 2005. Interspecific allometry of the brain and brain regions in parrots (Psittaciformes): comparisons with other birds and primates. Brain Behav Evol 65:40–59.

Iwaniuk AN, Gutierrez-Ibanez C, Pakan JMP, Wylie DR, 2010. Allometric scaling of the tectofugal pathway in birds. Brain Behav Evol 75:122–137.

Karten HJ. 1969. The Organization of the avian telencephalon and some speculations on the phylogeny of the amniote telencephalon. Ann N Y Acad Sci 167:164–179.

Karten HJ. 2007. *Gallus gallus*—Dataset. In: BrainMaps: an interactive multiresolution brain atlas. Accessed 20 November 2013. Available from: http://brainmaps.org.

Karten HJ, Hodos W, Nauta WJH, Revzin AM. 1973. Neural connections of the "visual wulst" of the avian telencephalon. Experimental studies in the pigeon (*Columba livia*) and owl (*Speotyto cunicularia*). J Comp Neurol 150:253–277.

Karten HJ, Cox K, Mpodozis J. 1997. Two distinct populations of tectal neurons have unique connections within the retinotectorotundal pathway of the pigeon (*Columba livia*). J Comp Neurol 387:449–465.

Karten HJ, Brzozowska-Prechtl A, Lovell PV, Tang DD, Mello CV, Wang H, Mitra PP. 2013. Digital atlas of the zebra finch (*Taeniopygia guttata*) brain: a high resolution photo atlas. J Comp Neurol 521:3702–3715.

Keary N, Voss J, Lehmann K, Bischof H-J, Löwel S. 2010. Optical imaging of retinotopic maps in a small songbird, the zebra finch. PLoS ONE 5:e11912.

Knudsen EI. 2002. Instructed learning in the auditory localization pathway of the barn owl. Nature 417:322–328.

Koshiba M, Yohda M, Nakamura S. 2005. Topological relation of chick thalamofugal visual projections with hyper pallium revealed by three color tracers. Neurosci Res 52: 235–242.

Lee J-Y, Holden LA, Djamgoz MBA. 1997. Effects of ageing on spatial aspects of the pattern electroretinogram in male and female quail. Vision Res 37:505–514.

Letelier J-C, Marín G, Sentis E, Tenreiro A, Fredes F, Mpodozis J. 2004. The mapping of the visual field onto the dorsolateral tectum of the pigeon (*Columba livia*) and its relations with retinal specializations. J Neurosci Methods 132:161–168.

Lisney TJ, Collin SP. 2008. Retinal ganglion cell distribution and spatial resolving power in elasmobranchs. Brain Behav Evol 72:59–77.

Lisney TJ, Iwaniuk AN, Bandet MV, Wylie DR. 2012a. Eye shape and retinal topography in owls (Aves: Strigiformes). Brain Behav Evol 79:218–236.

Lisney TJ, Iwaniuk AN, Kolominsky J, Bandet MV, Corfield JR, Wylie DR. 2012b. Interspecifc variation in eye shape and retinal topography in seven species of galliform bird (Aves: Galliformes: Phasianidae). J Comp Physiol A 198: 717–731.

Lisney TJ, Stecyk K, Kolominsky J, Schmidt BK, Corfield JR, Iwaniuk AN, Wylie DR. 2013. Ecomorphology of eye shape and retinal topography in waterfowl (Aves: Anseriformes: Anatidae) with different foraging modes. J Comp Physiol A 199:385–402.

Luksch H. 2003. Cytoarchitecture of the avian optic tectum: neuronal substrate for cellular computation. Rev Neurosci 14:85–106.

Luksch H, Karten HJ, Kleinfeld D, Wessel R. 2001. Chattering and differential signal processing in identified motion-sensitive neurons of parallel visual pathways in the chick tectum. J Neurosci 21:6440–6446.

Marín G, Letelier JC, Henny P, Sentis E, Farfán G, Fredes F, Pohl N, Karten H, Mpodozis J. 2003. Spatial organization of the pigeon tectorotundal pathway: an interdigitating topographic arrangement. J Comp Neurol 458:361–380.

Marín GJ, Durán E, Morales C, González-Cabrera C, Sentis E, Mpodozis J, Letelier JC. 2012. Attentional capture? Synchronized feedback signals from the isthmi boost retinal signals to higher visual areas. J Neurosci 32:1110–1122.

Martin G, Jarrett N, Tovey P, White C. 2005. Visual fields in flamingos: chick-feeding versus filter-feeding. Naturwissenschaften 92:351–354.

Martin GR. 1993. Producing the image. In: Zeigler HP, Bischof H-J, eds. Vision, brain, and behavior in birds. Cambridge, MA: MIT Press, pp. 5–24.

Martin GR. 2007. Visual fields and their functions in birds. J Ornithol 148:547–562.

Martin GR, Katzir G. 1995. Visual fields in ostriches. Nature 374:19–20.

Martin GR, Katzir G. 1999. Visual fields in short-toed eagles, *Circaetus gallicus* (Accipitridae), and the function of binocularity in birds. Brain Behav Evol 53:55–66.

Martin GR, Wilson K-J, Wild JM, Parsons S, Kubke MF, Corfield J. 2007. Kiwi forego vision in the guidance of their nocturnal activities. PLoS ONE 2:e198.

Maturana HR, Varela FJ. 1982. Color-opponent responses in the avian lateral geniculate: a study in the quail (*Coturnix coturnix japonica*). Brain Res 247:227–241.

Médina M, Repérant J, Ward R, Miceli D. 2004. Centrifugal visual system of *Crocodylus niloticus*: a hodological, histochemical, and immunocytochemical study. J Comp Neurol 468:65–85.

Miceli D, Peyrichoux J, Repérant J. 1975. The retino-thalamo-hyperstriatal pathway in the pigeon (*Columba livia*). Brain Res 100:125–131.

Miceli D, Repérant J, Rio J-P, Medina M. 1995. GABA immunoreactivity in the nucleus isthmo-opticus of the centrifugal visual system in the pigeon: a light and electron microscopic study. Vis Neurosci 12:425–441.

Miceli D, Repérant J, Bertrand C, Rio J-P. 1999. Functional anatomy of the avian centrifugal visual system. Behav Brain Res 98:203–210.

Miceli D, Repérant J, Ward R, Rio J-P, Jay B, Médina M, Kenigfest NB. 2008. Fine structure of the visual dorsolateral anterior thalamic nucleus of the pigeon (*Columba livia*): a hodological and GABA-immunocytochemical study. J Comp Neurol 507:1351–1378.

Moroney M, Pettigrew J. 1987. Some observations on the visual optics of kingfishers (Aves, Coraciformes, Alcedinidae). J Comp Physiol A 160:137–149.

Mpodozis J, Letelier J-C, Concha ML, Maturana H. 1995. Conduction velocity groups in the retino-tectal and retino-

thalamic visual pathways of the pigeon (*Columba livia*). Int J Neurosci 81:123–136.

Muchnick N, Hibbard E. 1980. Avian retinal ganglion cells resistant to degeneration after optic nerve lesion. Exp Neurol 68:205–216.

Müller J, Reisz RR. 2005. Four well-constrained calibration points from the vertebrate fossil record for molecular clock estimates. Bioessays 27:1069–1075.

Nalbach H-O, Wolf-Oberhollenzer F, Kirschfeld K. 1990. The pigeon's eye viewed through an ophthalmoscopic microscope: orientation of retinal landmarks and significance of eye movements. Vision Res 30:529–540.

Nickla DL, Gottlieb MD, Marin G, Rojas X, Britto LRG, Wallman J. 1994. The retinal targets of centrifugal neurons and the retinal neurons projecting to the accessory optic system. Vis Neurosci 11:401–409.

Norgren RB, Silver R. 1989a. Retinal projections in quail (*Coturnix coturnix*). Vis Neurosci 3:377–387.

Norgren RB, Silver R. 1989b. Retinohypothalamic projections and the suprachiasmatic nucleus in birds. Brain Behav Evol 34:73–83.

O'Leary DDM, Cowan WM. 1982. Further studies on the development of the isthmo-optic nucleus with special reference to the occurrence and fate of ectopic and ipsilaterally projecting neurons. J Comp Neurol 212:399–416.

Omi M, Harada H, Nakamura H. 2011. Identification of retinotectal projection pathway in the deep tectal laminae in the chick. J Comp Neurol 519:2615–2621.

Pakan JMP, Wylie DRW. 2006. Two optic flow pathways from the pretectal nucleus lentiformis mesencephali to the cerebellum in pigeons (*Columba livia*). J Comp Neurol 499:732–744.

Pakan JMP, Krueger K, Kelcher E, Cooper S, Todd KG, Wylie DRW. 2006. Projections of the nucleus lentiformis mesencephali in pigeons (*Columba livia*): a comparison of the morphology and distribution of neurons with different efferent projections. J Comp Neurol 495:84–99.

Pearson AK, Pearson OP. 1955. Natural history and breeding behavior of the tinamou, *Nothoprocta ornata*. Auk 72: 113–127.

Pettigrew J, Konishi M. 1976. Neurons selective for orientation and binocular disparity in the visual wulst of the barn owl (*Tyto alba*). Science 193:675–678.

Pettigrew JD, Dreher B, Hopkins CS, McCall MJ, Brown M. 1988. Peak density and distribution of ganglion cells in the retinae of microchiropteran bats: implications for visual acuity. Brain Behav Evol 32:39–56.

Rahman ML, Sugita S, Aoyama M, Sugita S. 2006. Number, distribution and size of retinal ganglion cells in the jungle crow (*Corvus macrorhynchos*). Anat Sci Int 81:253–259.

Rahman ML, Aoyama M, Sugita S. 2007a. Topography of ganglion cells in the retina of the duck (*Anas platyrhynchos var. domesticus*). Anim Sci J 78:286–292.

Rahman ML, Aoyama M, Sugita S. 2007b. Regional specialization of the tree sparrow *Passer montanus* retina: ganglion cell density and oil droplet distribution. Ornithol Sci 6:95–105.

Rahman ML, Kuroda K, Aoyama M, Sugita S. 2010. Regional specialization of the ganglion cell density in the retina of the Ostrich (*Struthio camelus*). Anim Sci J 81:108–115.

Ramón y Cajal S. 1909. Histologie du système nerveux de l'homme et des vertébrés. Paris, France: Maloine.

Remy M, Güntürkün O. 1991. Retinal afferents to the tectum opticum and the nucleus opticus principalis thalami in the pigeon. J Comp Neurol 305:57–70.

Repérant J, Ward R, Miceli D, Rio JP, Médina M, Kenigfest NB, Vesselkin NP. 2006. The centrifugal visual system of vertebrates: a comparative analysis of its functional anatomical organization. Brain Res Rev 52:1–57.

Repérant J, Médina M, Ward R, Miceli D, Kenigfest NB, Rio JP, Vesselkin NP. 2007. The evolution of the centrifugal visual system of vertebrates. A cladistic analysis and new hypotheses. Brain Res Rev 53:161–197.

Schmid KL, Wildsoet CF. 1998. Assessment of visual acuity and contrast sensitivity in the chick using an optokinetic nystagmus paradigm. Vision Res 38:2629–2634.

Schmidt A, Bischof H-J. 2001. Neurons with complex receptive fields in the stratum griseum centrale of the zebra finch (*Taeniopygia guttata castanotis* Gould) optic tectum. J Comp Physiol A 187:913–924.

Schmidt A, Engelage J, Bischof H-J. 1999. Single cell responses from the optic tectum of the zebra finch (*Taeniopygia guttata castanotis* Gould). J Comp Physiol A 185:69–79.

Schmitz C, Hof PR. 2000. Recommendations for straightforward and rigorous methods of counting neurons based on a computer simulation approach. J Chem Neuroanat 20:93–114.

Schulte M, Diekamp B, Manns M, Schwarz A, Valencia-Alfonso C, Kirsch JA. Güntürkün O, Folta K. 2006. Visual responses and afferent connections of the n. ventrolateralis thalami (VLT) in the pigeon (*Columba livia*). Brain Res Bull 68:285–292.

Shimizu T, Cox K, Karten HJ, Britto LRG. 1994. Cholera toxin mapping of retinal projections in pigeons (*Columba livia*), with emphasis on retinohypothalamic connections. Vis Neurosci 11:441–446.

Sorenson EM, Parkinson D, Dahl JL, Chiappinelli VA. 1989. Immunohistochemical localization of choline acetyltransferase in the chicken mesencephalon. J Comp Neurol 281:641–657.

Talbot CM, Marshall JN. 2011. The retinal topography of three species of coleoid cephalopod: significance for perception of polarized light. Philos Trans R Soc B Biol Sci 366:724–733.

Uchiyama H, Aoki K, Yonezawa S, Arimura F, Ohno H. 2004. Retinal target cells of the centrifugal projection from the isthmo-optic nucleus. J Comp Neurol 476:146–153.

Ullmann JFP, Moore BA, Temple SE, Fernández-Juricic E, Collin SP. 2012. The retinal wholemount technique: a window to understanding the brain and behaviour. Brain Behav Evol 79:26–44.

Vega-Zuniga T, Medina FS, Fredes F, Zuniga C, Severín D, Palacios AG, Karten HJ, Mpodozis J. 2013. Does nocturnality drive binocular vision? Octodontine rodents as a case study. PLoS ONE 8: e84199.

Vega-Zuniga T, Mpodozis J, Karten HJ, Marín G, Hain S, Luksch H. 2014. Morphology, projection pattern and neurochemical identity of Cajal's "centrifugal neurons": the cells of origin of the tectoventrogeniculate pathway in pigeon (*Columba livia*) and chicken (*Gallus gallus*). J Comp Neurol 522:2377–2396.

Verhaal J, Luksch H. 2013. Mapping of the receptive fields in the optic tectum of chicken (*Gallus gallus*) using sparse noise. PLoS ONE 8: e60782.

Verhaart WJ. 1971. Forebrain bundles and fibre systems in the avian brain stem. J Hirnforsch 13:39–64.

Walls GL. 1963. The vertebrate eye and its adaptive radiation. New York, NY: Hafner (reprinted from Cranbrook Institute of Science, Bloomfield Hills, MI, 1942).

Wang Y, Major DE, Karten HJ. 2004. Morphology and connections of nucleus isthmi pars magnocellularis in chicks (*Gallus gallus*). J Comp Neurol 469:275–297.

Wang Y, Luksch H, Brecha NC, Karten HJ. 2006. Columnar projections from the cholinergic nucleus isthmi to the optic tectum in chicks (*Gallus gallus*): a possible substrate for synchronizing tectal channels. J Comp Neurol 494:7–35.

Wässle H, Levick WR, Cleland BG. 1975. The distribution of the alpha type of ganglion cells in the cat's retina. J Comp Neurol 159:419–437.

Watanabe M. 1987. Synaptic organization of the nucleus dorsolateralis anterior thalami in the Japanese quail (*Coturnix coturnix japonica*). Brain Res 401:279–291.

Wathey JC, Pettigrew JD. 1989. Quantitative analysis of the retinal ganglion cell layer and optic nerve of the barn owl *Tyto alba*. Brain Behav Evol 33:279–292.

West MJ. 1999. Stereological methods for estimating the total number of neurons and synapses: issues of precision and bias. Trends Neurosci 22:51–61.

West MJ, Slomianka L, Gundersen HJG. 1991. Unbiased stereological estimation of the total number of neurons in the subdivisions of the rat hippocampus using the optical fractionator. Anat Rec 231:482–497.

Wilson M, Lindstrom SH. 2011. What the bird's brain tells the bird's eye: the function of descending input to the avian retina. Vis Neurosci 28:337–350.

Wizenmann A, Thanos S. 1990. The developing chick isthmo-optic nucleus forms a transient efferent projection to the optic tectum. Neurosci Lett 113:241–246.

Wood Casey A. 1917. The fundus oculi of birds, especially as viewed by the ophthalmoscope; a study in the comparative anatomy and physiology. Chicago, IL: The Lakeside Press.

Wright MW, Bowmaker JK. 2001. Retinal photoreceptors of paleognathous birds: the ostrich (*Struthio camelus*) and rhea (*Rhea americana*). Vision Res 41:1–12.

Wylie DRW, Gutierrez-Ibanez C, Pakan JMP, Iwaniuk AN. 2009. The optic tectum of birds: mapping our way to understanding visual processing. Can J Exp Psychol 63:328–338.

Zeil J, Nalbach G, Nalbach H-O. 1986. Eyes, eye stalks and the visual world of semi-terrestrial crabs. J Comp Physiol A 159:801–811.